

# Cold-water corals and hydrocarbon-rich seepage in the Pompeia Province (Gulf of Cádiz) — living on the edge

Blanca Rincón-Tomás<sup>1</sup>, Jan-Peter Duda<sup>2,3</sup>, Luis Somoza<sup>4</sup>, Francisco Javier González<sup>4</sup>, Dominik Schneider<sup>1</sup>, Teresa Medialdea<sup>4</sup>, Pedro Madureira<sup>5</sup>, Michael Hoppert<sup>1</sup>, and Joachim Reitner<sup>2,3</sup>

<sup>1</sup>Georg-August-University Göttingen, Institute of Microbiology and Genetics, Grisebachstraße 8, 37077 Göttingen, Germany

<sup>2</sup>Georg-August-University Göttingen, Göttingen Centre of Geosciences, Goldschmidtstraße 3, 37077 Göttingen, Germany

<sup>3</sup>Göttingen Academy of Sciences and Humanities, Theaterstraße 7, 37073 Göttingen, Germany

<sup>4</sup>Marine Geology Dept., Geological Survey of Spain, IGME, Ríos Rosas 23, 28003 Madrid, Spain

<sup>5</sup>Estrutura de Missão para a Extensão da Plataforma Continental. Rua Costa Pinto 165, 2770-047 Paço de Arcos, Portugal

Correspondence to: Blanca Rincón-Tomás (b.rincontomas@gmail.com)

**Abstract.** Azooxanthellate cold-water corals (CWCs) have a global distribution and have commonly been found in areas of active fluid seepage. The relationship between the CWCs and these fluids, however, is not well understood. This study aims at unraveling the relationship between CWC development and hydrocarbon-rich seepage in the Pompeia Province (Gulf of Cádiz, Atlantic Ocean). This region comprises mud volcanoes, coral ridges, and fields of coral mounds, which are all affected by the tectonically driven seepage of hydrocarbon-rich fluids. The type of seepage such as focused, scattered, diffused or eruptive, however, is tightly controlled by a complex system of faults and diapirs. Early diagenetic carbonates from the currently active Al Gacel MV exhibit  $\delta^{13}\text{C}$ -signatures down to  $-28.77$  ‰ VPDB, indicating biologically derived methane as the main carbon source. The same samples contained  $^{13}\text{C}$ -depleted lipid biomarkers diagnostic for archaea such as crocetane ( $\delta^{13}\text{C}$  down to  $-101.2$  ‰ VPDB) and PMI ( $\delta^{13}\text{C}$  down to  $-102.9$  ‰ VPDB), evidencing microbially mediated anaerobic oxidation of methane (AOM). This is further supported by next generation DNA sequencing data, demonstrating the presence of AOM related microorganisms (ANME archaea, sulfate-reducing bacteria) in the carbonate. Embedded corals in some of the carbonates and CWC fragments exhibit less negative  $\delta^{13}\text{C}$  values ( $-8.08$  to  $-1.39$  ‰ VPDB), pointing against the use of methane as the carbon source. Likewise, the absence of DNA from methane- and sulfide-oxidizing microbes in a sampled coral does not support a chemosynthetic lifestyle of these organisms. In the light of these findings, it appears that the CWCs benefit rather indirectly from hydrocarbon-rich seepage by using methane-derived authigenic carbonates as a substratum for colonization. At the same time, chemosynthetic organisms at active sites prevent coral dissolution and necrosis by feeding on the seeping fluids (i. e. methane, sulfate, hydrogen sulfide), allowing cold-water corals to colonize carbonates currently affected by hydrocarbon-rich seepage.

## 1. Introduction

Cold-water corals (CWCs) are a widespread, non-phylogenetic group of cnidarians that include hard skeleton scleractinian corals, soft-tissue octocorals, gold corals, black corals and hydrocorals (Roberts et al., 2006; Roberts et al., 2009; Cordes et al., 2016). Typically, they thrive at low temperatures ( $4 - 12$  °C) and occur in water depths of ca.  $50 - 4000$  m. CWCs are azooxanthellate and solely rely on their nutrition as energy and carbon sources (Roberts et al., 2009). Some scleractinian corals (e.g. *Lophelia pertusa*, *Madrepora oculata*, *Dendrophyllia cornigera*, *Dendrophyllia alternata*, *Eguchipsammia cornucopia*) are able to form colonies or even large carbonate

41 mounds (Rogers et al., 1999; Wienberg et al., 2009; Watling et al., 2011; Somoza et al., 2014). Large vertical  
42 mounds and elongated ridges formed by episodic growth of scleractinian corals (mainly *Lophelia pertusa*) are for  
43 instance widely distributed along the continental margins of the Atlantic Ocean (Roberts et al., 2009). These  
44 systems are of great ecological value since they offer sites for resting-, breeding-, and feeding for various  
45 invertebrates and fishes (Cordes et al., 2016 and references therein).

46 Several environmental forces influence the initial settling, growth, and decline of CWCs. These include, among  
47 others, an availability of suitable substrates for coral larvae settlement, low sedimentation rates, oceanographic  
48 boundary conditions (e.g. salinity, temperature and density of the ocean water) and a sufficient supply of nutrients  
49 through topographically controlled currents systems (e.g. Mortensen et al., 2001; Roberts et al., 2003; Thiem et  
50 al., 2006; Dorschel et al., 2007; Dullo et al., 2008; Van Rooij et al., 2011; Hebbeln et al., 2016). Alternatively, the  
51 “hydraulic theory” supports that CWC ecosystems may be directly fueled by fluid seepage, providing a source of  
52 sulfur compounds, nitrogen compounds, P, CO<sub>2</sub> and/or hydrocarbons (Hovland, 1990; Hovland and Thomsen,  
53 1997; Hovland et al., 1998; 2012). This relationship is supported by the common co-occurrence of CWC-mounds  
54 and hydrocarbon-rich seeps around the world, for example at the Hikurangi Margin in New Zealand (Liebetrau et  
55 al., 2010), the Brazil margin (e.g. Gomes-Sumida et al., 2004), the Darwin Mounds in northern Rockall Trough  
56 (Huvenne et al., 2009), the Kristin field on the Norwegian shelf (Hovland et al., 2012), the western Alborán Sea  
57 (Margreth et al., 2011), and the Gulf of Cádiz (e.g. Díaz-del-Río et al., 2003; Foubert et al., 2008). However,  
58 CWCs may also benefit rather indirectly from seepage. For instance, methane-derived authigenic carbonates  
59 (MDACs) formed through the microbially mediated anaerobic oxidation of methane (AOM; Suess & Whiticar,  
60 1989; Hinrichs et al., 1999; Thiel et al., 1999; Boetius et al., 2000; Hinrichs & Boetius, 2002) potentially provide  
61 hard substrata for larval settlement (e.g. Díaz-del-Río et al., 2003; Goedert & Peckmann, 2005; Van Rooij et al.,  
62 2011; Magalhães et al. 2012; Le Bris et al., 2016; Rueda et al., 2016). In addition, larger hydrocarbon-rich seepage  
63 related structures such as mud volcanoes and carbonate mud mounds act as morphological barriers favoring  
64 turbulent water currents that deliver nutrients to the corals (Roberts et al., 2009; Wienberg et al., 2009; Margreth  
65 et al., 2011; Vandorpe et al., 2016).

66 In the Gulf of Cádiz, most CWC occurrences are “coral graveyards” with only a few living corals that are situated  
67 along the Iberian and Moroccan margins. These CWC systems are typically associated with diapiric ridges, steep  
68 fault-controlled escarpments, and mud volcanoes (MVs) such as the Faro MV, Hesperides MV, Mekness MV, and  
69 MVs in the Pen Duick Mud Volcano Province (Foubert et al., 2008; Wienberg et al., 2009). MVs (and other  
70 conspicuous morphological structures in this region such as pockmarks) are formed through tectonically induced  
71 fluid flow (Pinheiro et al., 2003; Somoza et al., 2003; Medialdea et al., 2009; León et al., 2010; 2012). This is  
72 because of the high regional tectonic activity and high fluid contents of sediments in this area (mainly CH<sub>4</sub> and, to  
73 a lesser extent, H<sub>2</sub>S, CO<sub>2</sub>, and N<sub>2</sub>; Pinheiro et al., 2003; Hensen et al., 2007; González et al., 2012). However, the  
74 exact influence of fluid flow on CWC growth in this region remains elusive.

75 This study aims at elucidating the linkage between the present-day formation of MDACs and CWCs development  
76 along the Pompeia Province (**Fig. 1**), which encompasses mud volcanoes as the Al Gacel MV (León et al., 2012),  
77 diapiric coral ridges and mounds. We address this question by the combined analyses of high-resolution ROV  
78 underwater images, geophysical data (e.g. seabed topography, deep high-resolution multichannel seismic  
79 reflection data), and sample materials (petrographic features,  $\delta^{13}\text{C}$ - and  $\delta^{18}\text{O}$ -signatures of carbonates, lipid  
80 biomarkers and environmental 16s rDNA sequences of the prokaryotic microbial community). Based on our

81 findings, we propose an integrated model to explain the tempo-spatial and genetic relations between CWCs,  
82 chemosynthetic fauna and hydrocarbon-rich seepage in the study area.

## 83 **2. Materials and Methods**

84 This study is based on data and samples from the Pompeia Province that were collected during the Subvent-2  
85 cruise in 2014 aboard the R/V Sarmiento de Gamboa (**Fig. 1**). In order to elucidate the tempo-spatial and genetic  
86 relations between CWCs, chemosynthetic fauna and hydrocarbon-rich seepage in this area, we explored geological  
87 features by means of underwater imaging and geophysical data. Based on these findings, we sampled different  
88 geological structures (mud volcanoes and coral ridges). All samples were taken with a ROV arm and immediately  
89 stored at room temperature (petrographic analysis),  $-20$  degrees (stable isotopic analysis), and  $-80$  degrees  
90 (environmental DNA analysis). Subsequently, we conducted detailed analyses on selected sample materials from  
91 sites that were characterized by different types of seepage during sampling. These include sites at the Al Gacel  
92 MV (D10-R3, D10-R7, D11-R8) and the Northern Pompeia Coral Ridge (D03-B1) (**Fig. 1**).

### 93 **2.1. Geophysical survey**

94 Seabed topography of the studied sites was mapped by using an Atlas Hydrosweep DS (15 kHz and 320 beams)  
95 multibeam echosounder (MBES). Simultaneously, ultra-high resolution sub-bottom profiles were acquired with  
96 an Atlas Parasound P-35 parametric chirp profiler (0.5 – 6 kHz). Deep high-resolution multichannel seismic  
97 reflection data was obtained using an array of 7 SERCEL gi-guns (system composed of 250 + 150 + 110 + 45  
98 cubic inches) with a total of 860 cubic inches. The obtained data were recorded with an active streamer  
99 (SIG@16.3x40.175; 150 m length with 3 sections of 40 hydrophones each). The shot interval was 6 seconds and  
100 the recording length 5 seconds two-way travel time (TWT). Data processing (filtering and stacking) was performed  
101 on board with Hot Shots software.

### 102 **2.2. Video survey and analysis**

103 A remotely operated vehicle (ROV-6000 Luso) was used for photographic documentation (high definition digital  
104 camera, 1024x1024 pixel) and sampling. The ROV was further equipped with a STD/CTD-SD204 sensor (*in-situ*  
105 measurements of salinity, temperature, oxygen, conductivity, sound velocity and depth), HydroC<sup>TM</sup> sensors (*in-*  
106 *situ* measurements of CO<sub>2</sub> and CH<sub>4</sub>) and Niskin bottles (CH<sub>4</sub> concentrations).

### 107 **2.3. Petrographic analysis**

108 General petrographic analysis was performed on thin sections (ca. 60  $\mu$ m thickness) with a Zeiss SteREO  
109 Discovery.V8 stereomicroscope (transmitted- and reflected light) linked to an AxioCam MRc 5-megapixel camera.  
110 Additional detailed petrographic analysis of textural and mineralogical features was conducted on polished thin  
111 sections (ca. 30  $\mu$ m thickness) using a DM2700P Leica Microscope coupled to a DFC550 digital camera.  
112 Carbonate textures have been classified following Dunham (1962) and Embry & Klovan (1971).

### 113 **2.4. Stable isotopes ( $\delta^{13}\text{C}$ , $\delta^{18}\text{O}$ ) of carbonates**

114 Stable carbon and oxygen isotope measurements were conducted on ca. 0.7 mg carbonate powder obtained with a  
115 high precision drill ( $\varnothing$  0.8 mm). The analyses were performed with a Thermo Scientific Kiel IV carbonate device

116 coupled to a Finnigan Delta Plus gas isotope mass spectrometer. Accuracy and reproducibility were checked  
117 through the replicate analysis of a standard (NBS19) and reproducibility was better than 0.1 ‰. Stable carbon and  
118 oxygen isotope values are expressed in the standard  $\delta$  notation as per mill (‰) deviations relative to Vienna Pee  
119 Dee Belemnite (VPDB).

## 120 **2.5. Lipid biomarker analysis**

### 121 **2.5.1. Sample preparation**

122 All materials used were pre-combusted (500 °C for >3 h) and/or extensively rinsed with acetone prior to sample  
123 contact. A laboratory blank (pre-combusted sea sand) was prepared and analyzed in parallel to monitor laboratory  
124 contaminations.

125 The preparation and extraction of lipid biomarkers was conducted in orientation to descriptions in Birgel et al.  
126 (2006). Briefly, the samples were first carefully crushed with a hammer and internal parts were powdered with a  
127 pebble mill (Retsch MM 301, Haan, Germany). Hydrochloric acid (HCl; 10 %) was slowly poured on the powdered  
128 samples which were covered with dichloromethane (DCM)-cleaned water. After 24 h of reaction, the residues (pH  
129 3 – 5) were repeatedly washed with water and then lyophilized.

130 3 g of each residue was saponified with potassium hydroxide (KOH; 6 %) in methanol (MeOH). The residues were  
131 then extracted with methanol (40 mL, 2x) and, upon treatment with HCl (10 %) to pH 1, in DCM (40 mL, 2x) by  
132 using ultra-sonification. The combined supernatants were partitioned in DCM vs. water (3x). The total organic  
133 extracts (TOEs) were dried with sodium sulfate (NaSO<sub>4</sub>) and evaporated with a gentle stream of N<sub>2</sub> to reduce loss  
134 of low-boiling compounds (cf. Ahmed and George, 2004).

135 Fifty percent of each TOE was separated over a silica gel column (0.7 g Merck silica gel 60 conditioned with *n*-  
136 hexane; 1.5 cm i.d., 8 cm length) into (a) hydrocarbon (6 mL *n*-hexane), (b) alcohol (7 mL DCM/acetone, 9:1, v:v)  
137 and (c) carboxylic acid fractions (DCM/MeOH, 3:1, v:v). Only the hydrocarbons were subjected to gas  
138 chromatography–mass spectrometry (GC-MS).

### 139 **2.5.2. Gas chromatography–mass spectrometry (GC-MS)**

140 Lipid biomarker analyses of the hydrocarbon fraction were performed with a Thermo Scientific Trace 1310 GC  
141 coupled to a Thermo Scientific Quantum XLS Ultra MS. The GC was equipped with a capillary column  
142 (Phenomenex Zebron ZB-5MS, 30 m length, 250  $\mu$ m inner diameter, 0.25  $\mu$ m film thickness). Fractions were  
143 injected into a splitless injector and transferred to the column at 300 °C. The carrier gas was He at a flow rate of  
144 1.5 mL min<sup>-1</sup>. The GC oven temperature was ramped from 80°C (1 min) to 310 °C at 5 °C min<sup>-1</sup> (held for 20 min).  
145 Electron ionization mass spectra were recorded in full scan mode at an electron energy of 70 eV with a mass range  
146 of *m/z* 50 – 600 and scan time of 0.42 s. Identification of individual compounds was based on comparison of mass  
147 spectra and GC retention times with published data and reference compounds.

### 148 **2.5.3 Gas chromatography–combustion–isotope ratio mass spectrometer (GC-C-IRMS)**

149 Compound specific  $\delta^{13}\text{C}$  analyses were conducted with a Trace GC coupled to a Delta Plus IRMS via a  
150 combustion-interface (all Thermo Scientific). The combustion reactor contained CuO, Ni and Pt and was operated  
151 at 940°C. The GC was equipped with two serially linked capillary columns (Agilent DB-5 and DB-1; each 30 m  
152 length, 250  $\mu$ m inner diameter, 0.25  $\mu$ m film thickness). Fractions were injected into a splitless injector and

153 transferred to the GC column at 290°C. The carrier gas was He at a flow rate of 20 ml min<sup>-1</sup>. The temperature  
154 program was identical to the one used for GC-MS (see above). CO<sub>2</sub> with known δ<sup>13</sup>C value was used for internal  
155 calibration. Instrument precision was checked using a mixture of *n*-alkanes with known isotopic composition.  
156 Carbon isotope ratios are expressed as δ<sup>13</sup>C (‰) relative to VPDB.

## 157 **2.6. Amplicon sequencing of 16S rRNA genes**

### 158 **2.6.1. DNA extraction and 16S rRNA gene amplification**

159 Environmental DNA analyses of microbial communities were performed on a carbonate sample with embedded  
160 corals from the base of the Al Gacel MV (D10-R3), a carbonate sample from an active pockmark close to the  
161 summit of the Al Gacel MV (D10-R7), and a necrotic fragment of a living *Madrepora oculata* recovered from the  
162 Northern Pompeia Coral Ridge (D03-B1). About 1 – 4 g of sample material was first mashed with mortar and  
163 liquid nitrogen to fine powder. Three biological replicates were used per sample. Total DNA was isolated with a  
164 Power Soil DNA Extraction Kit (MO BIO Laboratories, Carlsbad, CA). All steps were performed according to the  
165 manufacturer's instructions.

166 Bacterial amplicons of the V3 – V4 region were generated with the primer set MiSeq\_Bacteria\_V3\_forward  
167 primer (5'-TCGTCGGCAGCGTCAGATGTGTATAAGAGACAGCCTACGGGNGGCWGCAG-3') and  
168 MiSeq\_Bacteria\_V4\_reverse primer (5'-  
169 GTCTCGTGGGCTCGGAGATGTGTATAAGAGACAGGACTACHVGGGTATCTAATCC-3'). Likewise,  
170 archaeal amplicons of the V3 – V4 region were generated with the primer set MiSeq\_Archaea\_V3\_forward primer  
171 (5'-TCGTCGGCAGCGTCAGATGTGTATAAGAGACAG-GGTGBCAGCCGCGGTAA-3') and  
172 MiSeq\_Archaea\_V4\_reverse primer (5'-GTCTCGTGGGCTCGGAGATGTGTATAAGAGACAG-  
173 CCCGCAATTYCTTTAAG-3'). 50 µl of the PCR reaction mixture for bacterial DNA amplification, contained  
174 1 U Phusion high fidelity DNA polymerase (Biozym Scientific, Oldendorf, Germany), 5% DMSO, 0.2 mM of  
175 each primer, 200 µM dNTP, 0.15 µl of 25 mM MgCl<sub>2</sub>, and 25 ng of isolated DNA. The PCR protocol for bacterial  
176 DNA amplification included (i) initial denaturation for 1 min at 98 °C, (ii) 25 cycles of 45 s at 98 °C, 45 s at 60 °C,  
177 and 30 s at 72 °C, and (iii) a final extension at 72 °C for 5 min. The PCR reaction mixture for archaeal DNA  
178 amplification was similarly prepared but contained instead 1 µl of 25 mM MgCl<sub>2</sub> and 50 ng of isolated DNA. The  
179 PCR protocol for archaeal DNA amplification included (i) initial denaturation for 1 min at 98 °C, (ii) 10 cycles of  
180 45 s at 98 °C, 45 s at 63 °C, and 30 s at 72 °C, (iii) 15 cycles of 45 s at 98 °C, 45 s at 53 °C, and 30 s at 72 °C, and  
181 (iv) a final extension at 72 °C for 5 min.

182 PCR products were checked by agarose gel electrophoresis and purified using the GeneRead Size Selection Kit  
183 (QIAGEN GmbH, Hilden, Germany).

### 184 **2.6.2. Data analysis and pipeline**

185 Illumina PE sequencing of the amplicons and further process of the sequence data were performed in the Göttingen  
186 Genomics Laboratory (Göttingen, Germany). After Illumina MiSeq processing, sequences were analyzed as  
187 described in Egelkamp et al. (2017) with minor modifications. In brief, paired-end sequences were merged using  
188 PEAR v0.9.10 (Zhang et al., 2014), sequences with an average quality score below 20 and containing unresolved  
189 bases were removed with QIIME 1.9.1 (Caporaso et al., 2010). Non-clipped reverse and forward primer sequences  
190 were removed by employing cutadapt 1.15 (Martin, 2011). USEARCH version 9.2.64 was used following the

191 UNOISE pipeline (Edgar, 2010). In detail, reads shorter than 380 bp were removed, dereplicated, and denoised  
192 with the UNOISE2 algorithm of USEARCH resulting in amplicon sequence variants (ASVs) (Callahan et al.,  
193 2017). Additionally, chimeric sequences were removed using UCHIME2 in reference mode against the SILVA  
194 SSU database release 132 (Yilmaz et al., 2014). Merged paired-end reads were mapped to chimera-free ASVs and  
195 an abundance table was created using USEARCH. Taxonomic classification of ASVs was performed with BLAST  
196 against the SILVA database 132. Extrinsic domain ASVs, chloroplasts, and unclassified ASVs were removed from  
197 the dataset. Sample comparisons were performed at same surveying effort, utilizing the lowest number of  
198 sequences by random subsampling (20,290 reads for bacteria, 13,900 reads for archaea).  
199 The paired-end reads of the 16S rRNA gene sequencing were deposited in the National Center for Biotechnology  
200 Information (NCBI) in the Sequence Read Archive SRP156750.

## 201 **3. Results**

### 202 **3.1. The Pompeia Province — geological settings**

203 The Pompeia Province is situated in the Gulf of Cádiz offshore Morocco, within the so-called Middle Moroccan  
204 Field (Ivanov et al., 2000) at water-depths between 860 and 1000 m (**Fig. 1**). It comprises the active Al Gacel  
205 MV (**Fig. 1, C**), another mud volcano which is extinct (further referred as extinct MV) and two east-west elongated  
206 ridges (Northern Pompeia Coral Ridge and Southern Pompeia Coral Ridge). Scattered coral-mounds surround the  
207 ridges with a smooth relief (**Fig. 1, B**). CWCs were observed on seismic profiles resting on all these morphological  
208 features. Detailed geological profiles and 3D images of these features are shown in **Figs. 2** and **3**.

209 The Al Gacel MV is a cone-shape structure, 107 m high and 944 m wide, with its summit at 762 m depth and  
210 surrounded by a 11 m deep rimmed depression (León et al., 2012) (**Fig. 1, C**). It is directly adjacent to the Northern  
211 Pompeia Coral Ridge (**Fig. 2, A–B**), which extends ca. 4 km in westward direction (**Fig. 2, A–B**) and it is  
212 terminated by the Pompeia Escarpment (**Fig. 1, B; Fig. 2, C**). High resolution seismic profiles of the Pompeia  
213 Escarpment show CWC build-ups (R1 to R4) with steep lateral scarps of ca. 40 m height (**Fig. 2, C**). This MV is  
214 of sub-circular shape and exhibits a crater at its top (**Fig. 2, A–B**).

215 Ultra-high resolution sub-bottom seismic profile crossing the Pompeia Province from northwest (NW) to southeast  
216 (SE) (**Fig. 3, A**), shows (i) the Al Gacel MV surrounded by bottom-current deposits, (ii) an up to 130 m high CWC  
217 framework, growing on top the Southern Pompeia Coral Ridge, and (iii) semi-buried CWC mounds surrounding  
218 the ridge in areas of low relief. These CWC mounds locally form smooth, up to 25 – 30 m high top-rounded reliefs  
219 that are exposed, but then taper downward below the seafloor (applying sound speeds of 1750 m/s in recent  
220 sediments). Additionally, a multichannel seismic profile following the same track but with higher penetration  
221 below the seafloor (**Fig. 3, B**) shows high amplitude reflections inside the Al Gacel cone and enhanced reflections  
222 at the top of the diapirs (yellow dotted-line in **Fig. 3, B**), pointing to the occurrence of gas (hydrocarbon)-charged  
223 sediments. It furthermore exhibits breaks in seismic continuity and diapiric structures at different depths below the  
224 Southern Pompeia Coral Ridge and the Al Gacel MV, evidencing a fault system (**Fig. 3, B**). These tectonic  
225 structures may promote the development of overpressure areas (OP in **Fig. 3, B**) and consequent upward fluid flow  
226 to the surface.

### 227 **3.2. ROV observation and measurements**

228 Submersible ROV surveys at the Al Gacel MV (**Fig. 1, C**) revealed the presence of dispersed pockmark  
229 depressions at the eastern (Dive 10, 790 m) and northern flanks (Dive 11, 760 – 825 m depth). These sites are  
230 characterized by focused but low intensity seafloor bubbling (e.g. **Fig. 4, B; Fig. 5, A**). Analysis of water samples  
231 revealed CH<sub>4</sub>-concentration up to 171 nM during Dive 10 and up to 192 nM during Dive 11 (Sánchez-Guillamón  
232 et al., 2015). Pockmarks were essentially formed by grey-olive mud breccia sediments and characterized by  
233 deposits of authigenic carbonates appearing in the center and edges, together with typical methane-seep related  
234 organisms (e.g. sulfide-oxidizing bacterial mats, chemosynthetic bivalves, siboglinid tubeworms) (**Fig. 4, B–C;**  
235 **Fig. 5**). Communities of non-chemosynthetic organisms (e.g. sponges, corals) were also found at pockmarks (**Fig.**  
236 **4, B–C; Fig. 5, C**), but were more abundant in places where no seepage was detected (**Fig. 4, A**).  
237 Observations with the submersible ROV at the Northern Pompeia Coral Ridge and the extinct MV (Dive 03)  
238 revealed widespread and abundant occurrences of dead scleractinian-corals (mainly *Madrepora oculata* and  
239 *Lophelia pertusa*) currently colonized by few living non-chemosynthetic organisms (e.g. *Corallium tricolor*, other  
240 octocorals, sea urchins) (**Fig. 6, B–D**). Locally, grey-black colored patches of sulfide-oxidizing bacterial mats  
241 surrounded by shells of chemosynthetic bivalves (*Lucinoma asapheus* and *Thysira vulcolutre*) were detected (**Fig.**  
242 **6, A**). CH<sub>4</sub>-seepage appeared to be less than at the Al Gacel MV, with concentrations of 80 – 83 nM.  
243 Water parameters display homogenous values between the four sampling sites (10 °C temperature, ca. 52 – 55 %  
244 dissolved oxygen, ca. 31 Kg/m<sup>3</sup> density) (**Table 1**).

### 245 **3.3. Petrography and stable isotopes signatures of carbonates ( $\delta^{18}\text{O}$ , $\delta^{13}\text{C}$ )**

246 Sample D10-R3 derives from a field of carbonates at the base of the Al Gacel MV which is inhabited by sponges  
247 and corals (**Fig. 4, A**). The sample is a framestone composed of deep water scleractinian corals (*Madrepora* and  
248 rare *Lophelia*) (**Fig. 7, A–B**). The corals are typically cemented by microbial automicrite (*sensu* Reitner et al.  
249 1995) followed by multiple generations of aragonite. A matrix of dark allomicrite (*sensu* Reitner et al. 1995) with  
250 oxidized framboidal pyrites and remains of planktonic foraminifera is restricted to few bioerosional cavities (ca.  
251 5%) in the skeletons of dead corals (**Fig. 8, A–B**).  $\delta^{13}\text{C}$  signatures of the matrix and cements range from –26.68 to  
252 –18.38 ‰, while the embedded coral fragments exhibit  $\delta^{13}\text{C}$  values between –5.58 and –2.09 ‰ (**Fig. 7, B; Table**  
253 **2**). The  $\delta^{18}\text{O}$  values generally range from +2.35 to +3.92 ‰ (**Fig. 9; Table 2**).

254 Sample D10-R7 was recovered from a pockmark on the eastern site of the Al Gacel MV that is influenced by  
255 active seepage (**Fig. 3, C**). It consists of black carbonate and exhibits a strong hydrogen sulfide (H<sub>2</sub>S) odor (**Fig.**  
256 **5, B; Fig. 7, C–D**). The top of this sample was inhabited by living octocorals (**Fig. 5, C**), while chemosymbiotic  
257 siboglinid worms were present on the lower surface (**Fig. 5, D**). The sample is characterized by a grey peloidal  
258 wackestone texture consisting of allomicrite with abundant planktonic foraminifers and few deep water miliolids.  
259 The sample furthermore exhibits some fractured areas which are partly filled by granular and small fibrous cement,  
260 probably consisting of Mg-calcite. Locally, light brownish crusts of microbial automicrite similar to ones in D10-  
261 R3 are present (see above). Framboidal pyrite is abundant and often arranged in aggregates (**Fig. 8, C–D**). The  
262 carbonate exhibits  $\delta^{13}\text{C}$  values ranging from –28.77 to –21.13 ‰ and  $\delta^{18}\text{O}$  values from +2.37 to +3.15 ‰ (**Fig. 9;**  
263 **Table 2**).

264 Sample D11-R8 comes from an area with meter-sized carbonate blocks at the summit of the Al Gacel MV (**Fig. 4,**  
265 **D**) and is mainly colonized by sponges and serpulid worms (**Fig. 7, E**). The sample generally exhibits a light grey  
266 mud- to wackestone texture consisting of allomicrite with few scleractinian-coral fragments and planktonic  
267 foraminifers (**Fig. 7, E–F**). The carbonate furthermore contains abundant quartz silt and, locally, pyrite

268 enrichments. A further prominent feature are voids that are encircled by dark grey halos and exhibit brownish  
269 margins (due to enrichments of very small pyrite crystals and organic matter, respectively).  $\delta^{13}\text{C}$  signatures of the  
270 matrix and cements range from  $-14.82$  to  $-14.74$  ‰, while embedded coral fragments exhibit  $\delta^{13}\text{C}$  values of  $-4.91$   
271 to  $-2.99$  ‰ (**Fig. 7, F; Table 2**).  $\delta^{18}\text{O}$  values generally range from  $+1.49$  to  $+5.60$  ‰ (**Fig. 9; Table 2**).  
272 Sample D03-B1 is a necrotic fragment of a living scleractinian coral (*Madrepora oculata*) recovered from the  
273 Northern Pompeia Coral Ridge (**Fig. 6, D; Fig. 7, G**). The coral-carbonate exhibits  $\delta^{13}\text{C}$  values ranging from  $-8.08$   
274 to  $-1.39$  ‰ and  $\delta^{18}\text{O}$  values from  $-0.31$  to  $+2.26$  ‰ (**Fig. 9; Table 2**).

### 275 **3.4. Lipid biomarkers and compound specific carbon isotope signatures**

276 The hydrocarbon fractions of the carbonate recovered from the active pockmark (D10-R7) mainly consist of the  
277 irregular, tail-to-tail linked acyclic isoprenoids 2,6,11,15-tetramethylhexadecane ( $\text{C}_{20}$ ; crocetane), 2,6,10,15,19-  
278 pentamethylcosane ( $\text{C}_{25}$ ; PMI), as well as of several unsaturated homologues of these compounds (**Fig. 10**).  
279 Additionally, it contains the regular, head-to-tail linked acyclic isoprenoid pristane ( $\text{C}_{19}$ ).

280 The hydrocarbon fraction of the carbonate recovered from the summit of the Al Gacel MV (D11-R8) is dominated  
281 by *n*-alkanes with chain-lengths ranging from  $\text{C}_{14}$  to  $\text{C}_{33}$  (maxima at *n*- $\text{C}_{16}$  and, subordinated, at *n*- $\text{C}_{20}$  and *n*- $\text{C}_{31}$ )  
282 (**Fig. 10**). The sample further contains pristane, crocetane, the head-to-tail linked acyclic isoprenoid phytane ( $\text{C}_{20}$ )  
283 and traces of PMI.

284 Crocetane and PMI exhibited strongly depleted  $\delta^{13}\text{C}$  values in the carbonate from the active pockmark (D10-R7)  
285 ( $-101.2$  ‰ and  $-102.9$  ‰, respectively), while they showed less depleted  $\delta^{13}\text{C}$  values in the carbonate from the  
286 summit of the volcano (D11-R8) ( $-57.2$  ‰ and  $-74.3$  ‰, respectively).  $\delta^{13}\text{C}$  values of *n*-alkanes in the carbonate  
287 D11-R8 (*n*- $\text{C}_{17-22}$ ) ranged between  $-30.8$  ‰ and  $-33.0$  ‰ (**Table 3**).

### 288 **3.5. Prokaryotic community structure**

289 Bacterial DNA (**Fig. 11, A**) from samples D10-R3 (authigenic carbonate, base of the Al Gacel MV) and D03-B1  
290 (*Madrepora oculata* fragment, Northern Pompeia Coral Ridge) mainly derives from taxa that typically thrive in  
291 the water-column (e. g. Actinobacteria, Acidobacteria, Chloroflexi, Bacteroidetes, Woeseiaceae, Dadabacteria,  
292 Kaiserbacteria, Poribacteria, Planctomycetes, Gemmatimonadetes). The sample D10-R3 furthermore contains  
293 bacterial DNA of the nitrite-oxidizing bacteria *Nitrospira sp.*, while the sample D03-B1 contains DNA of the  
294 bacterial taxa Verrucomicrobia, Enterobacteria, *Nitrosococcus*. Noteworthy, one amplicon sequence variant  
295 (ASV\_189) with low number of clustered sequences has been found in D03-B1, identified as a methanotrophic  
296 symbiont of *Bathymodiulus mauritanicus* (see Rodrigues et al., 2013).

297 Up to 50 % of bacterial DNA in sample D10-R7 (authigenic carbonate, top of the Al Gacel MV) derives from taxa  
298 that are commonly associated with fluid seepage and AOM, i.e. sulfide-oxidizing bacteria, sulfate-reducing  
299 bacteria (SRB) and methane-oxidizing bacteria. The most abundant are SRB taxa like SEEP-SRB1, SEEP-SRB2,  
300 *Desulfatiglans*, *Desulfobulbus* and *Desulfococcus*, which typically form consortia with ANME archaea.

301 Archaeal DNA (**Fig. 11, B**) from samples D10-R3 and D03-B1 mainly consist of *Cenarchaeum sp.*, which  
302 represents 70 – 90 %. *Candidatus Nitrosopumilus* is the second most abundant in both samples, representing 5 –  
303 20 %. In contrast, around 90 % of archaeal DNA in D10-R7 is related to ANME-1 and ANME-2 groups, in good  
304 concordance with the relative abundances of SRB DNA.

305 Details of the number of reads per taxa are shown in the supplementary data, **Tables 1 and 2**.



## 306 4. Discussion

### 307 4.1. Evidence of hydrocarbon-rich seepage affecting the Pompeia Province

308 Two-dimensional multichannel-seismic images show that the Pompeia Province is affected by fluid expulsion  
309 related to compressional diapiric ridges and thrust faults (**Fig. 3, B**), as it has been reported from other areas of the  
310 Gulf of Cádiz (Somoza et al., 2003; Van Rensbergen et al., 2005; Medialdea et al., 2009). There seem to be  
311 different types of fault-conduit systems that link the overpressure zones (OP) with the seafloor (**Fig. 3, B**),  
312 controlling both type and rate of seepage (e.g. eruptive, focused, diffused or dripping-like). Dripping-like refers to  
313 intermittent bubbling fluids. At the Al Gacel MV, conduits are for instance mainly linked to faults and a dense  
314 hydro-fracture network, allowing the migration of hydrocarbon-rich muds from the overpressure zone to the  
315 surface. During active episodes, eruptions lead to the formation of mud-breccia flows as observed in gravity cores  
316 (e.g. León et al., 2012). During rather dormant episodes, focused and dripping-like seepage predominates, forming  
317 pockmark features (**Fig. 4, B**).

318 Currently, the Al Gacel MV is affected by continuous and focused dripping-like seepages. These sites of active  
319 seepage are characterized by carbonates that are suspected to be methane-derived (e.g. sample D10-R7, **Fig. 4, B–**  
320 **C**). In-situ ROV-measurements and subsequent water sample analysis demonstrated high concentrations of CH<sub>4</sub>  
321 in fluids that were escaping upon removal of the carbonate D10-R7 from the active pockmark (171 nM; **Fig. 5, A**)  
322 (Sánchez-Guillamón et al., 2015). This association suggests a genetic relationship between hydrocarbon-rich  
323 seepage and the carbonate, as also evidenced by the low  $\delta^{13}\text{C}$ -values of the carbonates analyzed herein (down to  
324 ca.  $-30\text{‰}$ , **Fig. 9; Table 2**). Indeed, the grey peloidal texture of this sample resembles that of AOM-derived  
325 automicrites from the Black Sea that are related to micro-seepage of methane (cf. Reitner et al., 2005). The here  
326 observed isotopically depleted acyclic isoprenoids such as crocetane and PMI ( $\delta^{13}\text{C}$  values between ca.  $-103$  and  
327  $-57\text{‰}$ ; **Fig. 10; Table 3**) are typical fingerprints of AOM-associated Archaea (Hinrichs et al., 1999; Thiel et al.,  
328 1999, 2001; Peckmann et al., 2001; Peckmann & Thiel, 2004), which is also in good accordance with the high  
329 abundance of DNA related to ANME. At the same time, abundant framboidal pyrite in the carbonate (**Fig. 8, C–**  
330 **D**) and SRB-related DNA (**Fig. 11**) evidences microbial sulfate reduction in the environment. All these data clearly  
331 demonstrate that the carbonates have been formed via AOM, fueled by fluids from the underlying mud diapir.

332 Other carbonate samples from the Al Gacel MV (i.e. D10-R3 and D11-R8) probably have also been formed due  
333 to AOM as they are also isotopically depleted ( $\delta^{13}\text{C}$  values between ca.  $-25$  and  $-15\text{‰}$ , **Fig. 9, Table 2**). However,  
334 no active gas bubbling was observed during sampling, even though both samples still contain open voids which  
335 could form pathways for a continuous migration of fluids. In fact, several characteristics of these voids (e.g. dark  
336 halos formed by pyrite, brownish margins due to organic matter enrichments) are very similar to those of methane-  
337 derived carbonate conduits (cf. Reitner et al., 2015). This could imply that the intensity of hydrocarbon-rich  
338 seepage and consequently AOM, may have fluctuated through time. The relatively low dominance of crocetane  
339 and PMI in the carbonate D11-R8 from the summit of Al Gacel MV (**Fig. 10**), as well as their moderately depleted  
340  $\delta^{13}\text{C}$  values ( $-57.2\text{‰}$  and  $-74.3\text{‰}$ , respectively; **Table 3**), could be due to mixing effects and thus be in good  
341 accordance with varying intensities of AOM in the environment. Also, the presence of only few AOM-related  
342 DNA sequences (**Fig. 11**) and partly oxidized pyrites in the carbonate D10-R3 from the base of the Al Gacel MV  
343 (**Fig. 8, A–B**) are well in line with this scenario.

344 There is no evidence for eruptive extrusions of muddy materials at the coral ridges. In the Southern Pompeia Coral  
345 Ridge (**Fig. 3**), diapirs appear to rather promote an upward migration of hydrocarbon-rich fluids in a divergent

346 way throughout a more extensive seabed area. This results in a continuous and diffused seepage, which promotes  
347 the occurrence of AOM and the formation of MDACs at the base of the ridges, related to the sulphate-methane  
348 transition zone (SMTZ) (Boetius et al., 2000; Hinrichs and Boetius, 2002; González et al., 2012a). This is in good  
349 accordance with the detection of methane (80 – 83 nM) at the Northern Pompeia Coral Ridge and the presence of  
350 sulfide-oxidizing bacterial mats and shells of dead chemosynthetic bivalves at the western part of the ridge (**Fig.**  
351 **6, A**). Likewise, the CWC Mounds Field surrounding the Southern Pompeia Coral Ridge (**Fig. 3**) is thoroughly  
352 characterized by micro-seeps, due to ascending fluids from OPs through low-angle faults. This type of focused  
353 seepage may promote formation of MDAC pavements in deeper layers of the sediments (**Fig. 3**), similar to coral  
354 ridges along the Pen Duick Escarpment (Wehrmann et al., 2011). The generation of MDAC-hotspots at sites of  
355 such seepage also explain the geometry of the downward tapering cones (**Fig. 3**).

#### 356 **4.2. Ecological meaning of hydrocarbon-rich seepage for CWCs**

357 Our data suggests contemporaneous micro-seepage and CWC growth in the Pompeia Province (e.g. **Fig. 4, B**).  
358 This relationship has also been observed elsewhere, e.g. in North Sea and off Mid Norway (Hovland, 1990;  
359 Hovland & Thomsen, 1997), and the Angola margin (Le Guilloux et al., 2009). However, scleractinian fragments  
360 recovered from the Al Gacel MV (embedded in carbonates D10-R3 and D11-R8, from the base and summit of the  
361 volcano, respectively) and the Northern Pompeia Coral Ridge (D03-B1, necrotic part of a living *Madrepora*  
362 *oculata*) displayed barely depleted  $\delta^{13}\text{C}$  values (ca.  $-8$  to  $-1$  ‰; **Fig. 9; Table 2**), close to the  $\delta^{13}\text{C}$  of marine  
363 seawater ( $0 \pm 3$  ‰, e.g. Hoefs, 2015). This does not support a significant uptake of methane-derived carbon by the  
364 CWCs and thus a direct trophic dependency as previously proposed (Hovland, 1990). Furthermore, the only DNA  
365 in sample D03-B1 that could be attributed to a potential methanotrophic endosymbiont (ASV\_189; Rodrigues et  
366 al., 2013) occurred in minor amounts and most likely represents contamination from the environment or during  
367 sampling. Taken together, there is no evidence that CWCs in the working area harbor microbial symbionts which  
368 potentially could utilize the hydrocarbon-rich fluids. More likely, the CWCs feed on a mixture of phytoplankton,  
369 zooplankton and dissolved organic matter as previously proposed for ones in other regions (Kiriakoulakis et al.,  
370 2005; Duineveld et al., 2007; Becker et al., 2009; Liebetrau et al., 2010). This is in good accordance with the  
371 presence of DNA from various common archaeal and bacterial taxa (e.g. Acidobacteria, Actinobacteria,  
372 Candidatus *Nitrosopumilus*, *Cenarchaeum* sp.) and some potential members of the corals' holobiont (e.g.  
373 Enterobacteria, Verrucomicrobia, *Nitrosococcus* sp.) (Sorokin, 1995; Rädercker et al., 2015; Webster et al., 2016)  
374 in sample D03-B1 (**Fig. 11**).

375 CWC development and hydrocarbon-rich seepage are consequently linked *via* the formation of MDAC deposits,  
376 which provide the hard substrata needed for CWC larval settlement (e.g. Díaz-del-Río et al., 2003; Van Rooij et  
377 al., 2011; Magalhães et al., 2012; Le Bris et al., 2016; Rueda et al., 2016). If too severe, however, fluid flow and  
378 associated metabolic processes can result in local conditions that are lethal to CWCs (see 4.3). Moreover, AOM  
379 fueled by fluid flow can also cause an entombment of the CWCs by MDACs (Wienberg et al., 2009, Wienberg &  
380 Titschack, 2015), as observed in D10-R3 and D11-R8 carbonates from the Al Gacel MV (**Figs. 7 and 9; Tables 2**  
381 **and 3**). It is therefore not surprising that large CWC systems in the Pompeia Province are always linked to  
382 structures that are affected by rather mild, non-eruptive seepage (i.e. the extinct MV, the coral ridges and the CWC  
383 Mound Fields: **Figs. 3 and 6**). The observation that these systems are in large parts “coral graveyards” (**Fig. 6, B–**  
384 **D**), similar to other areas in the Gulf of Cádiz (see Foubert et al., 2008; Wienberg et al., 2009), may be explained  
385 by a post-glacial decrease in current strength (Foubert et al., 2008). In the light of our findings, however, they

386 could also have been negatively affected by periods of intensive seepage during higher tectonic activity. Future  
387 studies are important to test this hypothesis in greater detail.

### 388 **4.3. Spatio-temporal co-existence of CWCs and chemosynthetic organisms — the buffer effect**

389 As discussed above, MDAC deposits are ecologically beneficial for CWCs, as they served as optimal substrata  
390 even when seepage is still present (e. g. Hovland, 1990; Hovland & Thomsen, 1997; Le Guilloux et al., 2009; this  
391 study). Severe hydrocarbon-rich seepage, however, is ecologically stressful for the corals. Particularly, fluid- and  
392 AOM-derived hydrogen sulfide is considered problematic because of its role in coral necrosis (Myers &  
393 Richardson, 2009; García et al., 2016) and carbonate dissolution effects (Wehrmann et al., 2011).

394 Hydrogen sulfides can efficiently be buffered through the reaction with Fe-(oxyhydro)-oxides or Fe<sup>2+</sup> dissolved in  
395 pore waters, ultimately forming pyrite (Wehrmann et al., 2011). Fe-(oxyhydro)-oxides nodules have previously  
396 been observed in the Iberian and Moroccan margins (González et al., 2009; 2012b), but not in the Pompeia  
397 Province. Instead, sulfide-oxidizing bacteria living in symbiosis with invertebrates (e.g. siboglinid worms:  
398 Petersen & Dubilier, 2009) (**Fig. 5, D**) and thriving in mats (**Fig. 4, C; Fig. 6, A**) were particularly prominent along  
399 this region. These microbes may form a biological buffer by withdrawing reduced sulfur species through their  
400 metabolic activity. Likewise, the consumption of methane and sulfate by AOM-microorganisms at active sites also  
401 contribute to CWCs colonization of the carbonates by reducing environmental acidification.

402 We propose that this biological buffer provides a further ecological linkage between hydrocarbon-rich seepage  
403 and cold-water corals along the Pompeia Province (“buffer effect model”: **Fig. 12**). This model explains the  
404 observed co-existence of non-chemosynthetic corals (e.g. on top of D10-R7 carbonate: **Fig. 5**) with AOM-  
405 microorganisms and chemosynthetic sulfide-oxidizing organisms at pockmark sites at the Al Gacel MV (**Fig. 12,**  
406 **A**). At the same time, it is in line with associations of sulfide-oxidizing bacterial mats, scleractinian corals, and  
407 other non-chemosynthetic octocorals at diapiric ridges and coral mounds in the Northern Pompeia Coral Ridge  
408 (**Fig. 12, B, C**). The impact and exact capacity of this biological buffer, however, remains elusive and must be  
409 evaluated in future studies.

## 410 **5. Conclusions**

411 The presence of cold-water corals related to hydrocarbon-seep structures like mud volcanoes and diapirs, is partly  
412 due to the irregular topography affecting bottom water-currents, which supply nutrients to the corals. Likewise,  
413 their tight-linkage to active hydrocarbon-rich seepage occurs by means of the production of methane-derived  
414 carbonates and how they provide the hard substrata cold-water corals need to develop. The discovery of methane-  
415 derived carbonates with embedded corals evidences the decline of coral colonization when the intensity of the  
416 fluid seepage increases or becomes more violent. Consequently, cold-water coral growth in these habitats depends  
417 directly on seepage intensity and how these fluids are drained onto the seafloor (i.e. eruptive, focused, diffused or  
418 dripping-like). Furthermore, cold-water corals rely on the microbial AOM-metabolism and sulfide oxidation to  
419 reduce seeped fluids in the environment, since they are harmful for the corals. This biological buffer is possibly  
420 crucial to keep conditions favorable for the growth of cold-water corals in the studied area, particularly in times  
421 of increased fluid seepage.

## 422 **Author contribution**

423 Blanca Rincón-Tomás, Dominik Schneider and Michael Hoppert carried out the microbial analysis. Jan-Peter  
424 Duda carried out the biomarker analysis. Luis Somoza and Teresa Medialdea processed seismic and bathymetric  
425 data. Pedro Madureira processed ROV data. Francisco Javier González and Joachim Reitner carried out the  
426 petrographic analysis. Joachim Reitner carried out the stable isotopic analysis. Blanca Rincón-Tomás prepared  
427 the manuscript with contributions from all co-authors.

#### 428 **Competing interests**

429 The authors declare that they have no conflict of interest.

#### 430 **Acknowledgments**

431 The authors thank the captain and the crew on board the R/V Sarmiento de Gamboa, as well as the UTM (Unidad  
432 de Tecnología Marina), that have been essential for the success of this paper. Data obtained on board is collected  
433 in the SUBVENT-2 cruise, which can be found in the IGME archive. This work was supported by the Spanish  
434 project SUBVENT (CGL2012-39524-C02) and the project EXPLOSEA (CTM2016-75947) funded by the Spanish  
435 Ministry of Science, Innovation and Universities.

#### 436 **References**

- 437 Ahmed, M. and George, S.C.: Changes in the molecular composition of crude oils during their preparation for GC  
438 and GC–MS analyses, *Org. Geochem.*, 35, 137–155, doi:10.1016/j.orggeochem.2003.10.002, 2004.
- 439 Becker, E. L., Cordes, E. E., Macko, S. A., and Fisher, C. R.: Importance of seep primary production to *Lophelia*  
440 *pertusa* and associated fauna in the Gulf of Mexico, *Deep-sea Res Pt I*, 56(5), 786–800,  
441 doi:10.1016/j.dsr.2008.12.006, 2009.
- 442 Birgel, D., Thiel, V., Hinrichs, K. U., Elvert, M., Campbell, K. A., Reitner, J., Farmer, J. D., and Peckmann, J.:  
443 Lipid biomarker patterns of methane-seep microbialites from the Mesozoic convergent margin of  
444 California, *Org. Geochem.*, 37(10), 1289–1302, doi:10.1016/j.orggeochem.2006.02.004, 2006.
- 445 Boetius, A., Ravensschlag, K., Schubert, C. J., Rickert, D., Widdel, F., Gieseke, A., Amann, R., Jørgensen, B. B.,  
446 Witte, U., and Pfannkuche, O.: A marine microbial consortium apparently mediating anaerobic oxidation  
447 of methane, *Nature*, 407 (6804), 623–626, doi:10.1038/35036572, 2000.
- 448 Callahan, B., MacMurdie, P. J., and Holmes, S. O.: Exact sequence variants should replace optional taxonomic  
449 units in marker-gene data analysis, *ISME J.*, 11, 2639–2643, doi:10.1038/ismej.2017.119, 2017.
- 450 Caporaso, J.G., Kuczynski, J., Stombaugh, J., Bittinger, K., Bushman, F.D., Costello, E.K., Fierer, N., González-  
451 Peña, A., Goodrich, J. K., Gordon, J. I., Huttley, G. A., Knights, D., Koenig, J. E., Lozupone, C. A.,  
452 McDonald, D., Muegge, B. D., Pirrung, M., Reeder, J., Sevinsky, J. R., Turnbaugh, P. J., Walters, W. A.,  
453 Widmann, J., Yatsunenko, T., Zaneveld, J., and Knight, R.: QIIME allows analysis of high-throughput  
454 community sequencing data, *Nat. Methods*, 7, 335–336, doi:10.1038/nmeth.f.303, 2010.
- 455 Cordes, E., Arnaud-Haond, S., Bergstad, O., da Costa Falcão, A. P., Freiwald, A., Roberts, J. M., and Bernal, P.:  
456 Cold water corals, in: *The First Global Integrated Marine Assessment, World Ocean Assessment I*, United  
457 Nations, Cambridge University Press, Cambridge, United Kingdom, 2016.

458 Díaz-del-Río, V., Somoza, L., Martínez-Frías, J., Mata, M. P., Delgado, A., Hernandez-Molina, F. J., ..., Vázquez,  
459 J. T.: Vast fields of hydrocarbon-derived carbonate chimneys related to the accretionary  
460 wedge/olistostrome of the Gulf of Cádiz, *Mar. Geol.*, 195, 177–200, doi:10.1016/S0025-3227(02)00687-  
461 4, 2003.

462 Dorschel, B., Hebbeln, D., Foubert, A., White, M., and Wheeler, A. J.: Hydrodynamics and cold-water coral facies  
463 distribution related to recent sedimentary processes at Galway Mound west of Ireland, *Mar. Geol.*, 244,  
464 184–195, doi:10.1016/j.margeo.2007.06.010, 2007.

465 Duineveld, G. C., Lavaleye, M. S., Bergman, M. J., De Stigter, H., and Mienis, F.: Trophic structure of a cold-  
466 water coral mound community (Rockall Bank, NE Atlantic) in relation to the near-bottom particle supply  
467 and current regime, *B. Mar. Sci.*, 81 (3), 449–467, 2007.

468 Dullo, W. C., Flögel, S., and Rüggerberg, A.: Cold-water coral growth in relation to the hydrography of the Celtic  
469 and Nordic European continental margin, *Mar. Ecol. Prog. Ser.*, 371, 165–176, doi:10.3354/meps07623,  
470 2008.

471 Dunham, R. J., 1962, Classification of carbonate rocks according to their depositional texture, in: Classification  
472 of Carbonate Rocks, Ham, W. E. (Eds.), American Association of Petroleum Geologists Memoir 1, Tulsa,  
473 OK, 108–121, 1962.

474 Edgar, R. C.: USEARCH. <http://www.drive5.com/usearch>. 2010.

475 Egelkamp, R., Schneider, D., Hertel, R., and Daniel, R.: Nitrile-Degrading Bacteria Isolated from Compost, *Front.*  
476 *Environ. Sci.*, 5, doi: 10.3389/fenvs.2017.00056, 2017.

477 Embry III, A. F., and Klován, J. E.: A late Devonian reef tract on northeastern Banks Island, NWT, *B. Can. Petrol.*  
478 *Geol.*, 19(4), 730–781, 1971.

479 Foubert, A., Depreiter, D., Beck, T., Maignien, L., Pannemans, B., Frank, N., Blamart, D., and Henriot, J.:  
480 Carbonate mounds in a mud volcano province off north-west Morocco: key to processes and controls,  
481 *Mar. Geol.*, 248, 74–96, doi: 10.1016/j.margeo.2007.10.012, 2008.

482 Garcia, G. D., Santos, E. D. O., Sousa, G. V., Zingali, R. B., Thompson, C. C., and Thompson, F. L.:  
483 Metaproteomics reveals metabolic transitions between healthy and diseased stony coral *Mussismilia*  
484 *braziliensis*, *Mol. Ecol.*, 25(18), 4632–4644, doi:10.1111/mec.13775, 2016.

485 Goedert, J. L., and Peckmann, J.: Corals from deep-water methane-seep deposits in Paleogene strata of Western  
486 Oregon and Washington, U.S.A., in: Cold-water corals and Ecosystems, Freiwald, A., and Roberts, J. M.  
487 (eds.), Springer-Verlag, Berlin Heidelberg, 27–40, 2005.

488 Gomes-Sumida, P.Y., Yoshinaga, M.Y., Saint-Pastous Madureira, L.A., and Hovland, M.: Seabed pockmarks  
489 associated with deep water corals off SE Brazilian continental slope, Santos Basin, *Mar. Geol.*, 207, 159–  
490 167, doi:10.1016/j.margeo.2004.03.006, 2004.

491 González, F. J., Somoza, L., Lunar, R., Martínez-Frías, J., Martín Rubí, J. A., Torres, T., Ortiz, J. E., Díaz-del-  
492 Río, V., Pinheiro, L. M., and Magalhães, V. H.: Hydrocarbon-derived ferromanganese nodules in  
493 carbonate mud mounds from the Gulf of Cádiz: mud-breccia sediments and clasts as nucleation sites,  
494 *Mar. Geol.*, 261, 64–81, doi:10.1016/j.margeo.2008.11.005, 2009.

495 González, F. J., Somoza, L., León, R., Medialdea, T., de Torres, T., Ortiz, J. E., Martínez-Frías, J., and Merinero,  
496 R.: Ferromanganese nodules and micro-hardgrounds associated with the Cádiz Contourite Channel (NE  
497 Atlantic): Palaeoenvironmental records of fluid venting and bottom currents, *Chem. Geol.*, 310–311, 56–  
498 78, doi: 10.1016/j.chemgeo.2012.03.030, 2012a.

499 González, F. J., Somoza, L., Medialdea, T., León, R., Torres, T., Ortiz, J. E., and Martín-Rubí, J. A.: Discovery of  
500 ferromanganese hydrocarbon-related nodules associated with the Meknes mud volcano (Western  
501 Moroccan margin). European Geoscience Union 2012 (EGU2012). Viena (Austria). Geophys. Res. Abs.  
502 vol. 14, EGU2012-12306, 2012b.

503 Hebbeln, D., Van Rooij, D., and Wienberg, C.: Good neighbours shaped by vigorous currents: cold-water coral  
504 mounds and contourites in the North Atlantic, *Mar. Geol.*, 378, 171–185,  
505 doi:10.1016/j.margeo.2016.01.014, 2016.

506 Hensen, C., Nuzzo, M., Hornibrook, E., Pinheiro, L.M., Bock, B., Magalhães, V.H., and Brückmann, W.: Sources  
507 of mud volcano fluids in the Gulf of Cádiz — indications for hydrothermal imprint, *Geochim.*  
508 *Cosmochim. Ac.*, 71 (5), 1232–1248, doi:10.1016/j.gca.2006.11.022, 2007.

509 Hinrichs, K. -U., and Boetius, A.: The anaerobic oxidation of methane: new insights in microbial ecology and  
510 biogeochemistry, in: *Ocean Margin Systems*, Wefer, G., Billett, D., Hebbeln, D., Jørgensen, B.B.,  
511 Schlueter, M., Van Weering, T. (Eds.), Springer-Verlag, Berlin, 457–477, 2002.

512 Hinrichs, K. -U., Hayes, J. M., Sylva, S. P., Brewer, P. G., and De Long, E. F.: Methane-consuming archaeobacteria  
513 in marine sediments, *Nature*, 398, 802–805, doi:10.1038/19751, 1999.

514 Hoefs, J.: *Stable Isotope Geochemistry*, Springer, Berlin, 2015.

515 Hovland, M.: Do carbonate reefs form due to fluid seepage?, *Terra Nova*, 2, 8–18, doi:10.1111/j.1365-  
516 3121.1990.tb00031.x, 1990.

517 Hovland, M., Jensen, S., and Indreien, T.: Unit pockmarks associated with *Lophelia* coral reefs off mid-Norway:  
518 more evidence of control by ‘fertilizing’ bottom currents, *Geo-Mar. Lett.*, 32 (5–6), 545–554,  
519 doi:10.1007/s00367-012-0284-0, 2012.

520 Hovland, M., Mortensen, P. B., Brattgard, T., Strass, P., and Rokoengen, K.: Ahermatypic coral banks off mid-  
521 Norway: evidence for a link with seepage of light hydrocarbons, *Palaios*, 13, 189–200, doi:10.1043/0883-  
522 1351(1998)013<0189:ACBOME>2.0.CO;2, 1998.

523 Hovland, M., and Thomsen, E.: Cold-water corals — are they hydrocarbon seep related?, *Mar. Geol.*, 137, 159–  
524 164, doi:10.1016/S0025-3227(96)00086-2, 1997.

525 Huvenne, V. A., Masson, D. G., and Wheeler, A. J.: Sediment dynamics of a sandy contourite: the sedimentary  
526 context of the Darwin cold-water coral mounds, Northern Rockall Trough, *Int. J. Earth Sci.*, 98 (4), 865–  
527 884, doi: 10.1007/s00531-008-0312-5, 2009.

528 Ivanov, M. K., Akhmetzhanov, A. M., and Akhmanov, G. G.: Multidisciplinary study of geological processes on  
529 the North East Atlantic and Western Mediterranean Margins, in: *Ioc. Tech. S.*, 56, UNESCO, 2000.

530 Kiriakoulakis, K., Fisher, E., Wolff, G. A., Freiwald, A., Grehan, A., and Roberts, J. M.: Lipids and nitrogen  
531 isotopes of two deep-water corals from the North-East Atlantic: initial results and implications for their  
532 nutrition, in: *Cold-Water Corals and Ecosystems*, Freiwald, A., Roberts, J. M. (Eds.), Erlangen Earth  
533 Conf., Springer, Germany, 715–729, 2005.

534 Le Bris, N., Arnaud-Haond, S., Beaulieu, S., Cordes, E. E., Hilario, A., Rogers, A., van de Gaever, S., and  
535 Watanabe, H.: Hydrothermal Vents and Cold Seeps, in: *The First Global Integrated Marine Assessment*,  
536 United Nations, Cambridge University Press, Cambridge, United Kingdom, 2016.

537 Le Guilloux, E., Olu, K., Bourillet, J. F., Savoye, B., Iglésias, S. P., and Sibuet, M.: First observations of deep-sea  
538 coral reefs along the Angola margin, *Deep-sea Res. Pt. II*, 56, 2394–2403,  
539 doi:10.1016/j.dsr2.2009.04.014, 2009.

540 Liebetrau, V., Eisenhauer, A., and Linke, P.: Cold seep carbonates and associated cold-water corals at the  
541 Hikurangi Margin, New Zealand: new insights into fluid pathways, growth structures and geochronology,  
542 Mar. Geol., 272, 307–318, doi:10.1016/j.margeo.2010.01.003, 2010.

543 León, R., Somoza, L., Medialdea, T., Vázquez, J. T., González, F. J., López-González, N., Casas, D., del Pilar  
544 Mata, M., del Fernández-Puga, C., Giménez-Moreno, C. J., and Díaz-del-Río, V.: New discoveries of  
545 mud volcanoes on the Moroccan Atlantic continental margin (Gulf of Cádiz): morpho-structural  
546 characterization, Geo-Mar. Lett., 32, 473–488, doi:10.1007/s00367-012-0275-1, 2012.

547 Magalhães, V. H., Pinheiro, L. M., Ivanov, M. K., Kozlova, E., Blinova, V., Kolganova, J., Vasconcelos, C.,  
548 McKenzie, J. A., Bernasconi, S. M., Kopf, A., Díaz-del-Río, V., González, F. J., and Somoza, L.:  
549 Formation processes of methane-derived authigenic carbonates from the Gulf of Cádiz, Sediment. Geol.,  
550 243–244, 155–168, doi:10.1016/j.sedgeo.2011.10.013, 2012.

551 Margreth, S., Gennari, G., Rüggeberg, A., Comas, M. C., Pinheiro, L. M., and Spezzferri, S.: Growth and demise  
552 of cold-water coral ecosystems on mud volcanoes in the West Alboran Sea: The messages from planktonic  
553 and benthic foraminifera, Mar. Geol., 282, 26–39, doi:10.1016/j.margeo.2011.02.006, 2011.

554 Martin, M.: Cutadapt removes Adapter Sequences from High-Throughput Sequencing Reads, EMBnet.journal, 10–  
555 12, doi: 10.14806/ej.17.1.200, 2011.

556 Medialdea, T., Somoza, L., Pinheiro, L. M., Fernández-Puga, M. C., Vázquez, J. T., León, R., Ivanov, M. K.,  
557 Magalhães, V., Díaz-del-Río, V., and Vegas, R.: Tectonics and mud volcano development in the Gulf of  
558 Cádiz, Mar. Geol., 261, 48–63, doi:10.1016/j.margeo.2008.10.007, 2009.

559 Mortensen, P. B., Hovland, M. T., Fossa, J. H., and Furevik, D. M.: Distribution, abundance and size of *Lophelia*  
560 *pertusa* coral reefs in mid Norway in relation to seabed characteristics, J. Mar. Biol. Assoc. UK, 81, 581–  
561 597, doi:10.1017/S002531540100426X, 2001.

562 Myers, J.L., and Richardson, L.L.: Adaptation of cyanobacteria to the sulfide-rich microenvironment of black band  
563 disease of coral, FEMS Microbiol. Ecol., 67, 242–251, doi:10.1111/j.1574-6941.2008.00619.x, 2009.

564 Peckmann, J., Reimer, A., Luth, U., Luth, C., Hansen, B.T., Heinicke, C., Hoefs, J., and Reitner, J.: Methane-  
565 derived carbonates and authigenic pyrite from the northwestern Black Sea, Mar. Geol., 177, 129–150,  
566 doi:10.1016/S0025-3227(01)00128-1, 2001.

567 Peckmann, J., and Thiel, V.: Carbon cycling at ancient methane-seeps, Chem. Geol., 205 (3), 443–467,  
568 doi:10.1016/j.chemgeo.2003.12.025, 2004.

569 Petersen, J. M., and Dubilier, N.: Methanotrophic symbioses in marine invertebrates, Env. Microbiol. Rep., 1(5),  
570 319–335, doi:10.1111/j.1758-2229.2009.00081.x, 2009.

571 Pinheiro, L. M., Ivanov, M. K., Sautkin, A., Akhmanov, G., Magalhães, V. H., Volkonskaya, A., Monteiro, J. H.,  
572 Somoza, L., Gardner, J., Hamouni, N., and Cunha, M. R.: Mud volcanism in the Gulf of Cádiz: results  
573 from the TTR-10 cruise, Mar. Geol., 195, 131–151, doi:10.1016/S0025-3227(02)00685-0, 2003.

574 Rädercker, N., Pogoreutz, C., Voolstra, C. R., Wiedenmann, J., and Wild, C.: Nitrogen cycling in corals: The key  
575 to understanding holobiont functioning?, Trends Microbiol., 23 (8), 490–497,  
576 doi:10.1016/j.tim.2015.03.008, 2015.

577 Reitner, J., Gauret, P., Marin, F., and Neuweiler, F.: Automicrites in a modern marine microbialite. Formation  
578 model via organic martices (Lizard Island, Great Barrier Reef, Australia), Bull.-Inst. Oceanogr. Monaco,  
579 14, 237–263, 1995.

580 Reitner, J., Peckmann, J., Blumenberg, M., Michaelis, W., Reimer, A., and Thiel, V.: Concretionary methane-seep  
581 carbonates and associated microbial communities in Black Sea sediments, *Palaeogeogr., Palaeoclimatol.,*  
582 *Palaeocl.*, 227, 18–30, doi:10.1016/j.palaeo.2005.04.033, 2005.

583 Roberts, J. M., Long, D., Wilson, J. B., Mortensen, P. B., and Gage, J. D.: The cold-water coral *Lophelia pertusa*  
584 (Scleractinia) and enigmatic seabed mounds along the north-east Atlantic margin: are they related?, *Mar.*  
585 *Pollut. Bull.*, 46, 7–20, doi:10.1016/S0025-326X(02)00259-X, 2003.

586 Roberts, J. M., Wheeler, A. J., and Freiwald, A.: Reefs of the deep: the biology and geology of cold-water coral  
587 ecosystems, *Science*, 312 (5773), 543–547, doi:10.1126/science.1119861, 2006.

588 Roberts, J. M., Wheeler, A., Freiwald, A., and Cairns, S. (Eds.): Cold-water corals: the biology and geology of  
589 deep-sea coral habitats, Cambridge University Press, Cambridge, United Kingdom, 2009.

590 Rodrigues, C. F., Cunha, M. R., Génio, L., and Duperron, S.: A complex picture of associations between two host  
591 mussels and symbiotic bacteria in the Northeast Atlantic, *Naturwissenschaften*, 100, 21–31,  
592 doi:10.1007/s00114-012-0985-2, 2013.

593 Rogers, A. D.: The Biology of *Lophelia pertusa* (Linnaeus 1758) and other Deep-Water Reef-Forming Corals and  
594 Impacts from Human Activities, *Int. Rev. Hydrobiol.*, 84 (4), 315–406, doi:10.1002/iroh.199900032,  
595 1999.

596 Rueda, J. L., González-García, E., Krutzky, C., López-Rodríguez, J., Bruque, G., López-González, N., Palomino,  
597 D., Sánchez, R. F., Vázquez, J. T., Fernández-Salas, L. M., and Díaz-del-Río, V.: From chemosynthetic-  
598 based communities to cold-water corals: Vulnerable deep-sea habitats of the Gulf of Cádiz, *Mar.*  
599 *Biodiver.*, 46, 473–482, doi:10.1007/s12526-015-0366-0, 2016.

600 Sánchez-Guillamón, O., García, M. C., Moya-Ruiz, F., Vázquez, J. T., Palomino, D., Fernández-Puga, M. C., and  
601 Sierra, A.: A preliminary characterization of greenhouse gas (CH<sub>4</sub> and CO<sub>2</sub>) emissions from Gulf of Cádiz  
602 mud volcanoes, VIII Symposium MIA15, 2015.

603 Somoza, L., Ercilla, G., Urgorri, V., León, R., Medialdea, T., Paredes, M., González, F. J., and Nombela, M. A.:  
604 Detection and mapping of cold-water coral mounds and living *Lophelia* reefs in the Galicia Bank, Atlantic  
605 NW Iberia margin, *Mar. Geol.*, 349, 73–90, doi:10.1016/j.margeo.2013.12.017, 2014.

606 Somoza, L., León, R., Ivanov, M. Fernández-Puga, M. C., Gardner, J. M., Hernández-Molina, F. J., Pinheiro, L.  
607 M., Rodero, J., Lobato, A., Maestro, A., Vázquez, J. T., Medialdea, T., and Fernández-Salas, L. M.:  
608 Seabed morphology and hydrocarbon seepage in the Gulf of Cádiz mud volcano area: Acoustic imagery,  
609 multibeam and ultra-high resolution seismic data, *Mar. Geol.*, 195, 153–176, doi:10.1016/S0025-  
610 3227(02)00686-2, 2003.

611 Sorokin, Y. I.: Coral reef ecology, Springer, Germany, 1995.

612 Suess, E. and Whiticar, M. J.: Methane-derived CO<sub>2</sub> in pore fluids expelled from the Oregon subduction zone,  
613 *Palaeogeogr., Palaeoclimatol., Palaeocl.*, 71, 119–136, doi:10.1016/0031-0182(89)90033-3, 1989.

614 Thiel, V., Peckmann, J., Seifert, R., Wehrung, P., Reitner, J., and Michaelis, W.: Highly isotopically depleted  
615 isoprenoids: molecular markers for ancient methane venting, *Geochim. Cosmochim. Ac.*, 63, 3959–3966,  
616 doi:10.1016/S0016-7037(99)00177-5, 1999.

617 Thiel, V., Peckmann, J., Richnow, H.-H., Luth, U., Reitner, J., and Michaelis, W.: Molecular signals for anaerobic  
618 methane oxidation in Black Sea seep carbonates and a microbial mat, *Mar. Chem.* 73, 97–112,  
619 doi:10.1016/S0304-4203(00)00099-2, 2001.



620 Thiem, Ø., Ravagnan, E., Fosså, J. H., and Berntsen, J.: Food supply mechanisms for cold- water corals along a  
621 continental shelf edge, *J. Marine Syst.*, 26, 1481–1495, doi:10.1016/j.jmarsys.2005.12.004, 2006.

622 Vandorpe, T., Martins, I., Vitorino, J., Hebbeln, D., García-García, M., and Van Rooij, D.: Bottom currents and  
623 their influence on the sedimentation pattern in the El Arraiche mud volcano province, southern Gulf of  
624 Cádiz, *Mar. Geol.*, 378, 114–126, doi:10.1016/j.margeo.2015.11.012, 2016.

625 Vandorpe, T., Wienberg, C., Hebbeln, D., Van den Berghe, M., Gaide, S., Wintersteller, P., and Van Rooij, D.:  
626 Multiple generations of buried cold-water coral mounds since the Early-Middle Pleistocene Transition in  
627 the Atlantic Moroccan Coral Province, southern Gulf of Cádiz, *Palaeogeogr., Palaeoclimatol., Palaeocl.*,  
628 485, 293–304, doi:10.1016/j.palaeo.2017.06.021, 2017.

629 Van Rensbergen, P., Depreiter, D., Pannemans, B., Moerkerke, G., Van Rooij, D., Marsset, B., Akhmanov, G.,  
630 Blinova, V., Ivanov, M., Rachidi, M., Magalhães, V., Pinheiro, L., Cunha, M., and Henriët, J.P.: The  
631 Arraiche mud volcano field at the Moroccan Atlantic slope, Gulf of Cádiz, *Mar. Geol.*, 219, 1–17,  
632 doi:10.1016/j.margeo.2005.04.007, 2005.

633 Van Rooij, D., Blamart, D., De Mol, L., Mienis, F., Pirlet, H., Whermann, L. M., ..., Henriët, J. -P.: Cold-water  
634 coral mounds on the Pen Duick Escarpment, Gulf of Cádiz: The MiCROSYSTEMS project approach,  
635 *Mar. Geol.*, 282, 102–117, doi:10.1016/j.margeo.2010.08.012, 2011.

636 Watling, L., France, S. C., Pante, E., and Simpson, A.: Biology of Deep-Water Octocorals, in: *Advances in Marine*  
637 *Biology Volume 60*, Lesser, M. (Eds.), Academic Press, London, United Kingdom, 41–122, 2011.

638 Webster, N. S., Negri, A. P., Botté, E. S., Laffy, P. W., Flores, F., Noonan, S., Schmidt, C., and Uthicke, S.: Host-  
639 associated coral reef microbes respond to the cumulative pressures of ocean warming and ocean  
640 acidification *Sci. Rep.-UK*, 6, doi:10.1038/srep19324, 2016.

641 Wheeler, A. J., Beyer, A., Freiwald, A., de Haas, H., Huvenne, V. A., Kozachenko, M., Olu-Le Roy, K.,  
642 and Opderbecke, J.: Morphology and environment of cold-water coral carbonate mounds on the NW  
643 European margin, *Int. J. Earth Sci.*, 96, 37–56, doi:10.1007/s00531-006-0130-6, 2007.

644 Wehrmann, L. M. Templer, S. P., Brunner, B., Bernasconi, S. M., Maignien, L., and Ferdelman, T. G.: The imprint  
645 of methane seepage on the geochemical record an early diagenetic processes in cold-water coral mounds  
646 on Pen Duick Escarpment, Gulf of Cádiz, *Mar. Geol.*, 118–137, doi:10.1016/j.margeo.2010.08.005, 2011.

647 Wienberg, C., Hebbeln, D., Fink, H. G., Mienis, F., Dorschel, B., Vertino, A., López-Correa, M., and Freiwald,  
648 A.: Scleractinian cold-water corals in the Gulf of Cádiz—first clues about their spatial and temporal  
649 distribution, *Deep-sea Res. Pt. I*, 56 (10), 1873–1893, doi:10.1016/j.dsr.2009.05.016, 2009.

650 Wienberg, C., and Titschack, J.: Framework-forming scleractinian cold-water corals through space and time: a  
651 late Quaternary North Atlantic perspective, in: *Marine Animal Forests: The Ecology of Benthic*  
652 *Biodiversity Hotspots*, Rossi, S., Bramanti, L., Gori, A., and Orejas, C. (Eds.), Springer, Cham,  
653 Switzerland, 1–34, 2015.

654 Yilmaz, P., Parfrey, L.W., Yarza, P., Gerken, J., Pruese, E., Quast, C., Schweer, T., Peplies, J., Ludwig, W., and  
655 Glöckner, F. O.: The SILVA and ‘All-species Living Tree Project (LTP)’ taxonomic frameworks, *Nucleic*  
656 *Acids Res.*, 42, D643–D648, doi:10.1093/nar/gkt1209, 2014.

657 Zhang, J., Kobert, K., Flouri, T., and Stamatakis, A.: PEAR: a fast and accurate Illumina Paired-End reAd  
658 merger, *Bioinformatics*, 30 (5), 614–620, doi:10.1093/bioinformatics/btt593, 2014.

659  
660

661 **Table 1.** *In-situ* water variables measured during sampling with ROV sensors.

	<b>D10-R3</b>	<b>D10-R7</b>	<b>D11-R8</b>	<b>D03-B1</b>
Temperature (°C)	10.07	10.5	10.02	10.04 – 10.05
Depth (m)	850 – 890	791	763	829
Conductivity (mS/cm)	39.13 – 39.62	39.05 – 39.43	-	-
Salinity (ppt)	-	-	35.56 – 35.86	35.67 – 35.91
Saturation of dissolved oxygen (%)	53.64 – 54.69	54.02 – 54.35	51.95 – 53.92	52.46 – 56.22
Dissolved oxygen (mg/l)	4.81 – 4.90	4.85 – 4.88	4.66 – 4.84	4.71 – 5.09
Density (kg/m <sup>3</sup> )	31.03 – 31.42	30.94 – 31.24	30.92 – 31.08	31.26 – 31.41

662  
663  
664  
665  
666  
667  
668  
669  
670  
671  
672  
673  
674  
675  
676  
677  
678  
679  
680  
681  
682  
683  
684  
685  
686

687 **Table 2.** Stable carbon and oxygen isotopes ( $\delta^{13}\text{C}$ ,  $\delta^{18}\text{O}$ ) of samples from the Al Gacel MV and the Northern  
 688 Pompeia Coral Ridge.

Location	Sample	Origin of the carbonate	Identification number in Fig. 7	$\delta^{18}\text{O}$ (‰)	$\delta^{13}\text{C}$ (‰)
Al Gacel MV	D10-R3	Coral skeleton	1	2.35	-5.58
		Authigenic carbonate	2	3.37	-20.07
			3	3.60	-26.68
			4	3.70	-20.79
			5	3.45	-22.43
			6	3.80	-20.70
			7	3.28	-2.23
		Authigenic carbonate	8	3.83	-25.16
			9	3.63	-25.29
			10	3.91	-18.38
			11	3.60	-24.18
			12	3.55	-25.34
			13	3.56	-25.15
		Authigenic carbonate	14	3.50	-2.09
			15	3.92	-21.89
	D10-R7	Authigenic carbonate	21	2.90	-26.36
			22	3.15	-28.77
			23	2.94	-22.91
			24	2.67	-21.13
			25	2.37	-24.70
26			2.56	-23.60	
Coral skeleton		16	1.49	-4.91	
		17	2.13	-2.99	
		18	1.74	-4.22	
		19	5.60	-14.82	
Authigenic carbonate	20	5.55	-14.74		
	D03-B1	Coral skeleton	1.1	-0.38	-7.93
1.2			-0.86	-7.77	
1.3			-0.51	-7.35	
1.5			1.15	-5.26	
1.4			-1.03	-8.08	
1.6			0.69	-5.96	
1.7			0.54	-6.42	

690 **Table 2.** Continued

Location	Sample	Origin of the carbonate	Identification number in Fig. 7	$\delta^{18}\text{O}$ (‰)	$\delta^{13}\text{C}$ (‰)
Northern Pompeia Coral Ridge	D03-B1	Coral skeleton	3.1	1.59	-2.08
			3.2	-0.31	-6.27
			3.3	-0.89	-6.78
			3.4	-0.94	-6.73
			3.5	1.84	-2.21
			3.6	2.26	-1.39
			3.7	1.74	-2.87

691

692

693 **Table 3.** Stable carbon isotopic composition ( $\delta^{13}\text{C}$ ) of selected lipid biomarkers (in **Figure 10**). (\*) Please note  
694 that crocetane in D11-R8 coelutes with phytane. n.d. = not detected.

Compound	D10-R7 (‰)	D11-R8 (‰)
<i>n</i> -C <sub>17</sub>	n.d.	-33.0
<i>n</i> -C <sub>18</sub>	n.d.	-31.8
<i>n</i> -C <sub>19</sub>	n.d.	-31.1
<i>n</i> -C <sub>20</sub>	n.d.	-30.8
<i>n</i> -C <sub>21</sub>	n.d.	-31.5
<i>n</i> -C <sub>22</sub>	n.d.	-31.7
Crocetane*	-101.2	-57.2
PMI	-102.9	-74.3

695

696

697

698

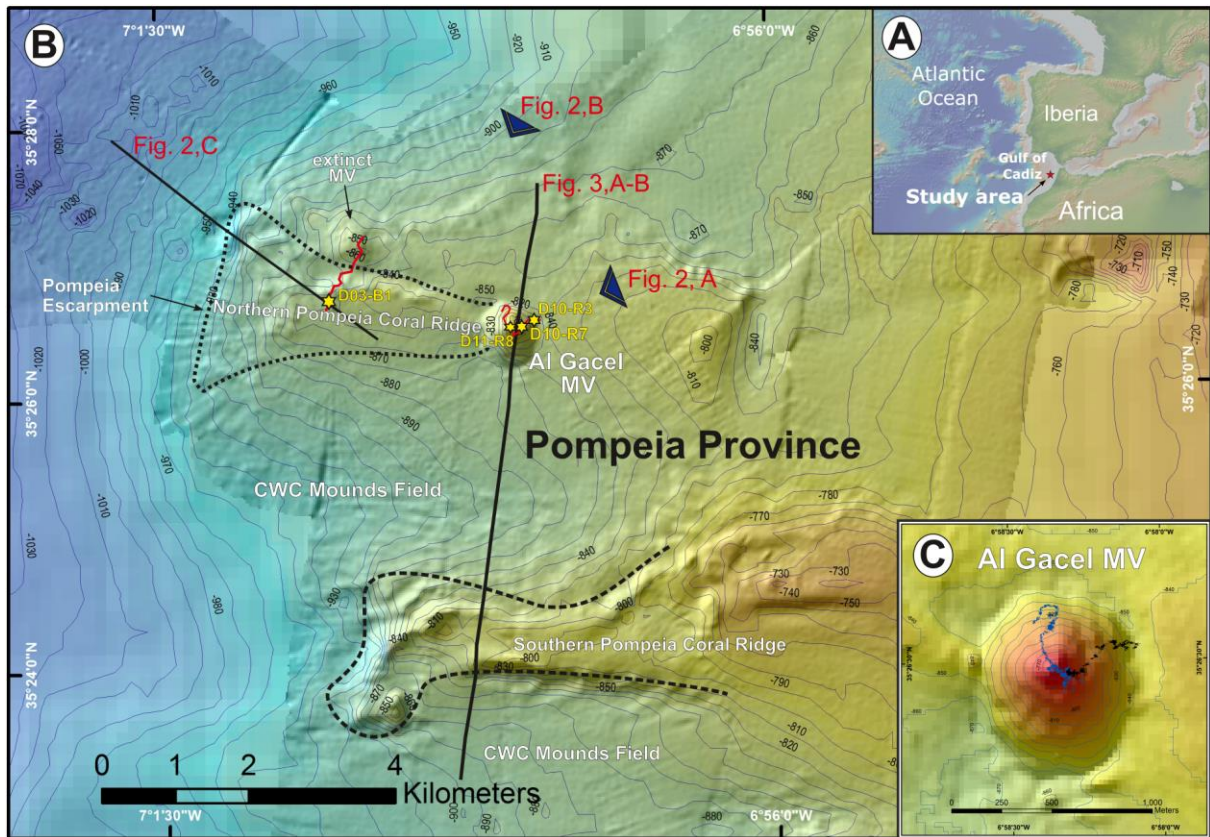
699

700

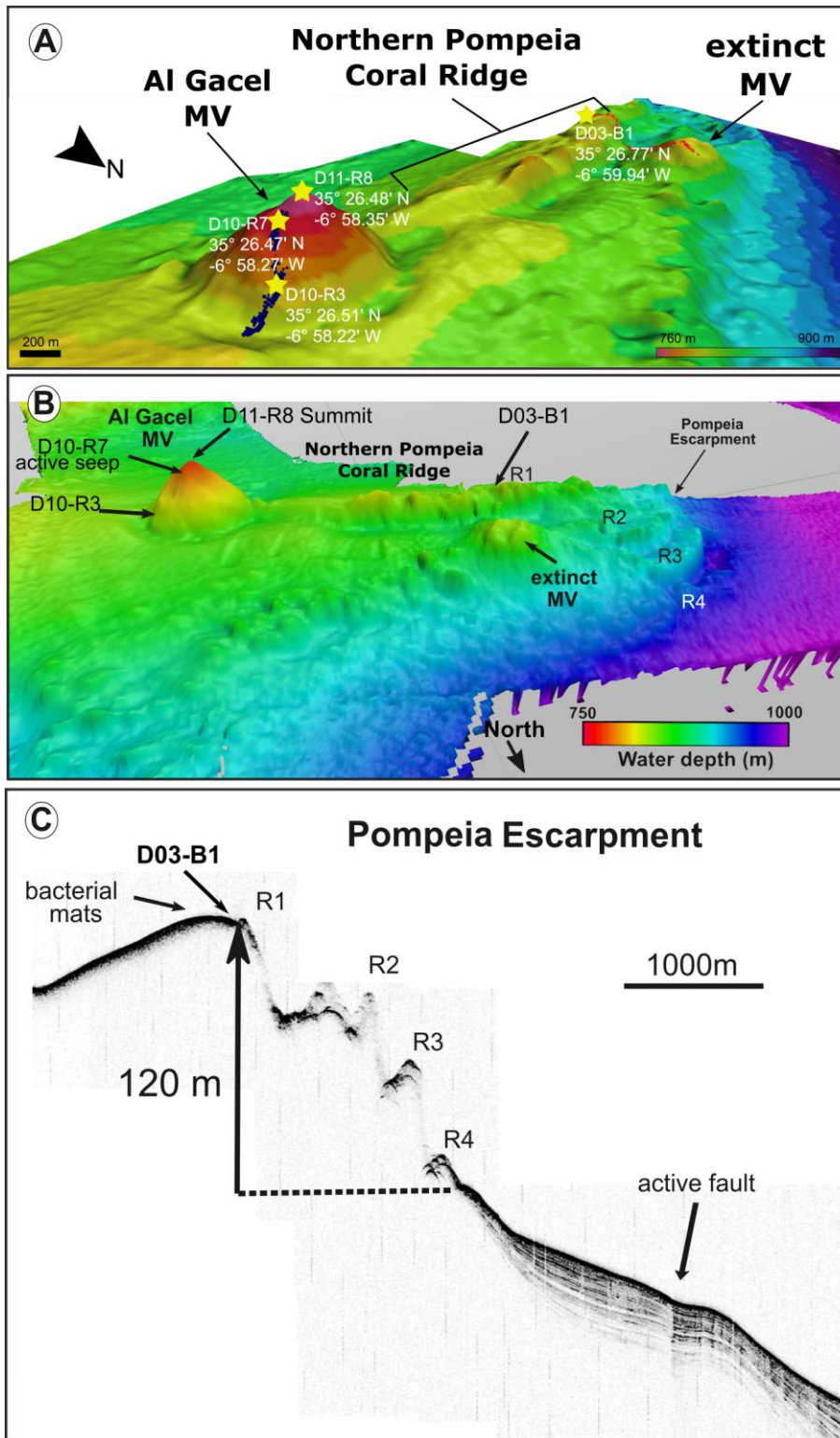
701

702

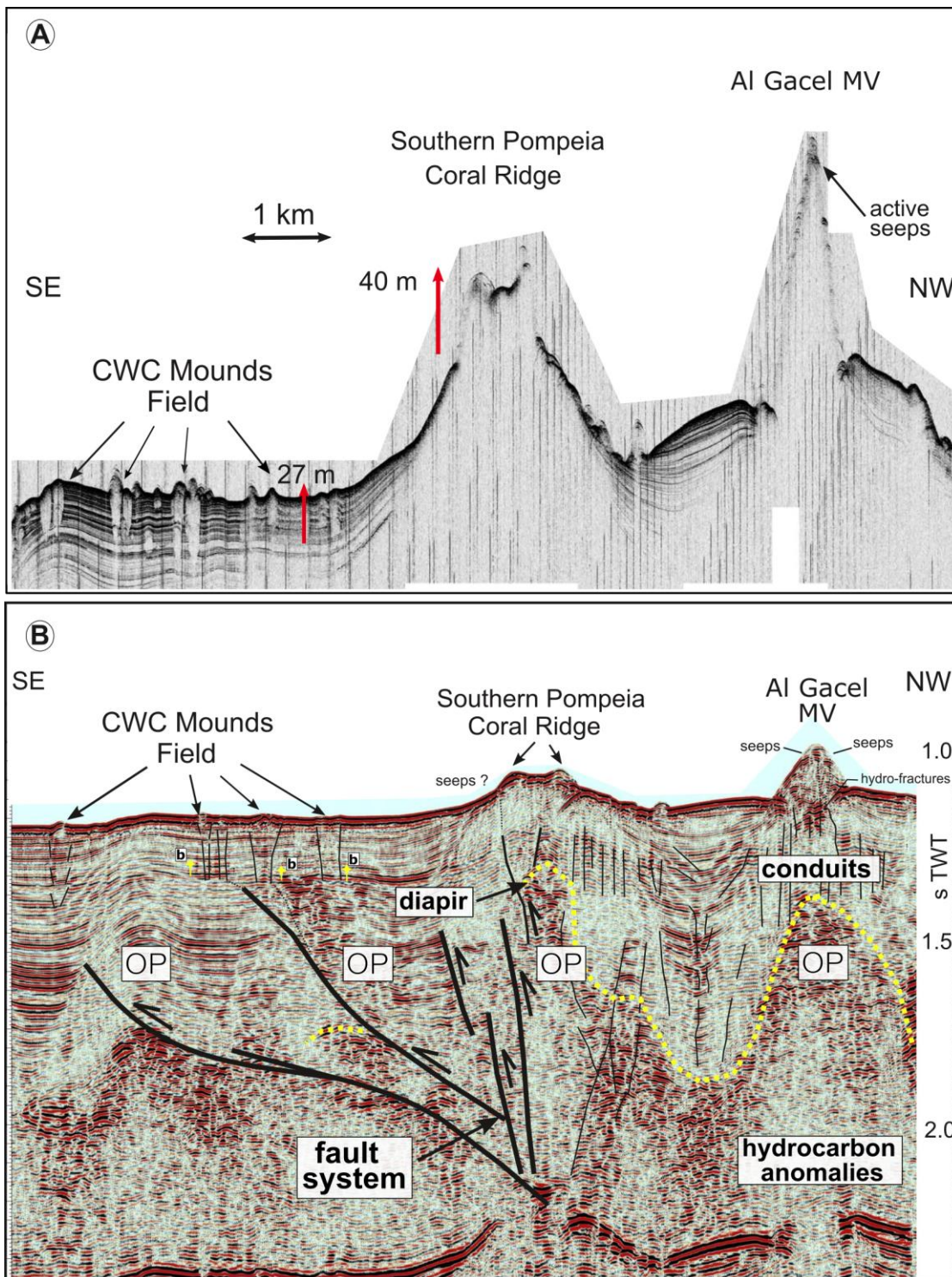
703



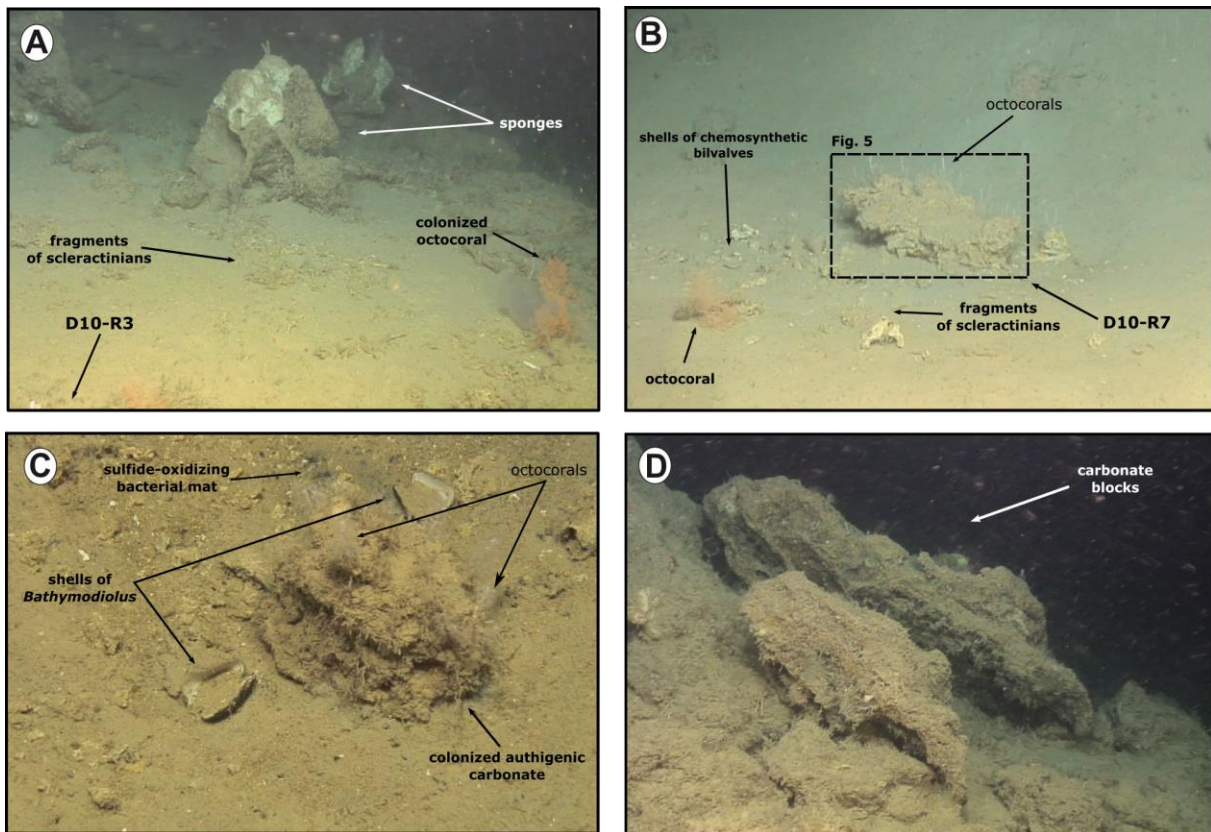
704  
 705 **Figure 1.** Bathymetric map of the study area. **A:** location of the Gulf of Cádiz between Spain, Portugal and  
 706 Morocco. The study area is marked with a red star; **B:** the Pompeia Province including its different morphological  
 707 features. Red lines indicate ROV-paths, yellow stars mark sampling sites; **C:** detailed map of the Al Gacel MV  
 708 including pathways of Dive 10 and 11 (black and blue lines, respectively). Further details of the area are provided  
 709 in **Figs. 2** and **3**.



710  
 711 **Figure 2.** Bathymetric and seismic maps showing morphological features in northern Pompeia Province. **A–B:**  
 712 bathymetric maps showing the Al Gacel MV, the Northern Pompeia Coral Ridge and the extinct MV. Yellow stars  
 713 mark sampling sites. **C:** ultra-high seismic profile of the Pompeia Escarpment, westwards of the Northern Pompeia  
 714 Coral Ridge.



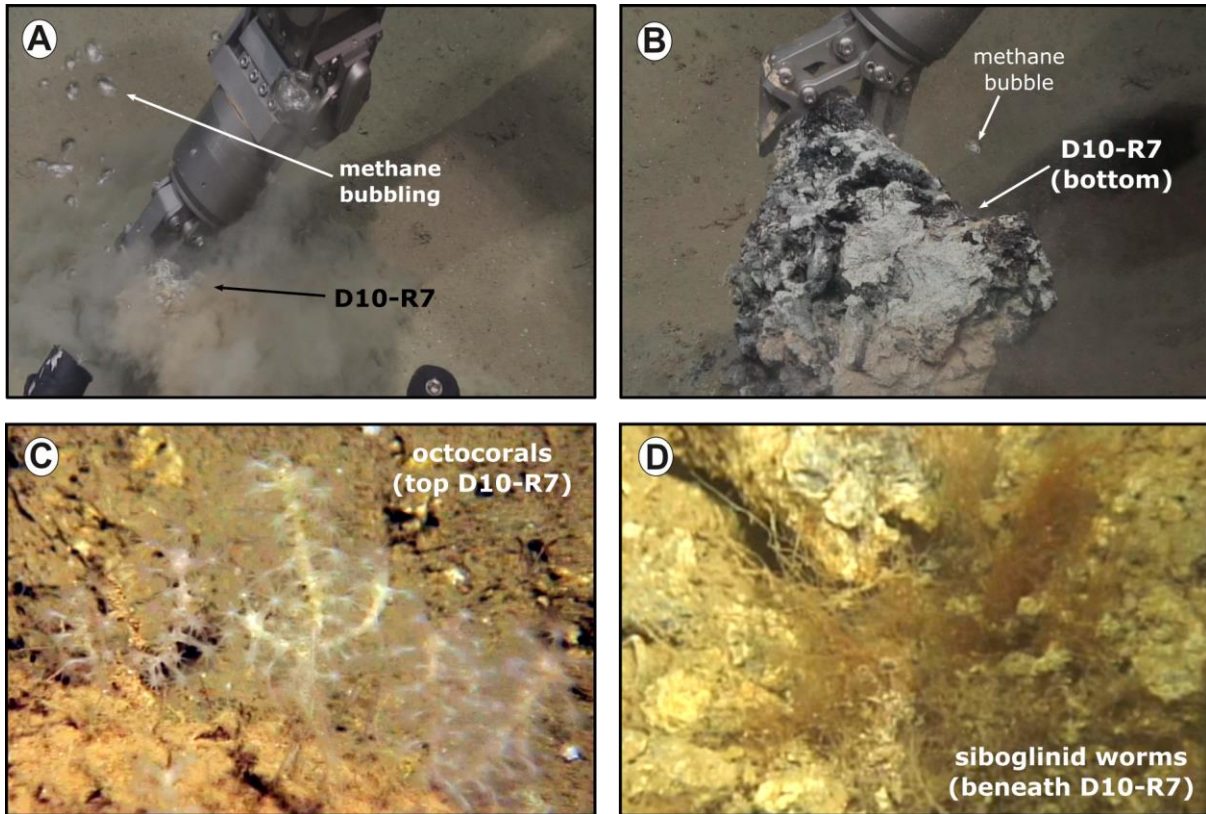
715  
 716 **Figure 3.** Ultra-high resolution (A) and multichannel (B) seismic profiles showing geological features in southern  
 717 Pompeia Province. Note mud diapirism has been described in this area (Vandorpe et al., 2017). OP = overpressure  
 718 zone.



719  
 720  
 721  
 722  
 723  
 724  
 725  
 726

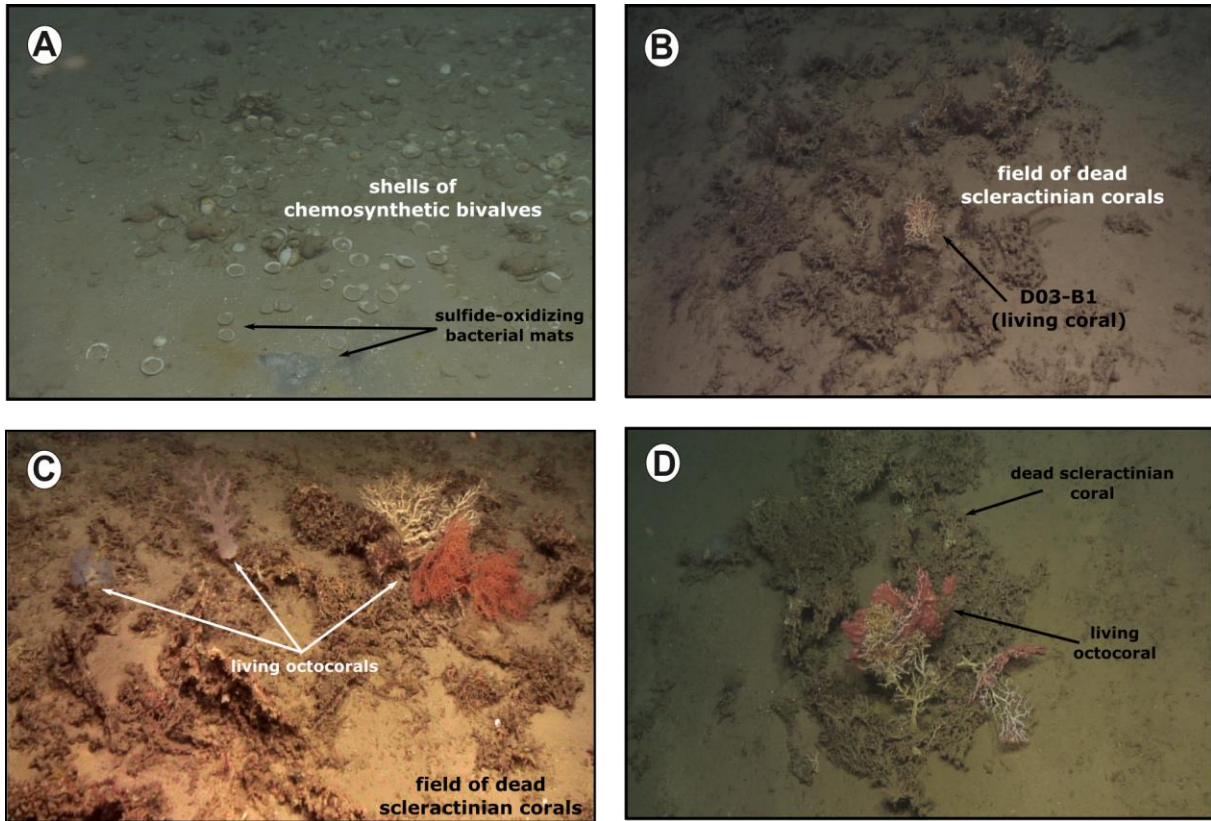
**Figure 4:** ROV still frames from the Al Gacel MV (Dives 10 and 11). **A:** eastern side of the volcano, displaying a field of sponges, corals and carbonates; **B–C:** active pockmark sites on the east side of the volcano, displaying authigenic carbonate surrounded by shells of chemosynthetic bivalves, fragments of scleractinian and octocorals, as well as sulfide-oxidizing bacterial mats; **D:** metric-sized carbonate blocks located in a slope at the summit of the volcano.





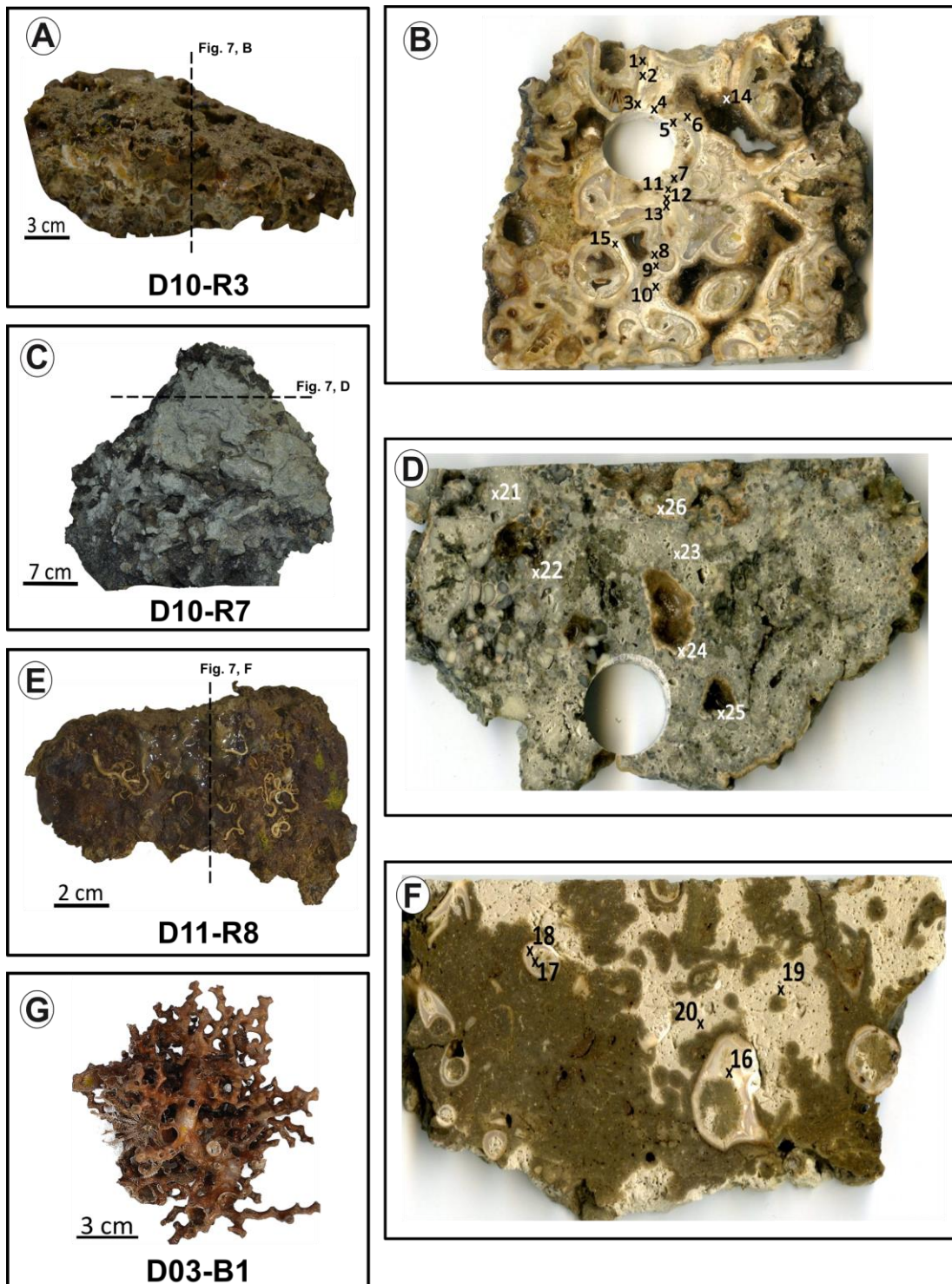
727  
 728  
 729  
 730  
 731  
 732  
 733

**Figure 5:** ROV still frames from the active pockmark site shown in Fig. 4, B. A–B: release of bubbles while sampling; C: detailed photograph of the octocorals on top of the carbonate; D: detailed still frame from siboglinid worms beneath the carbonate.



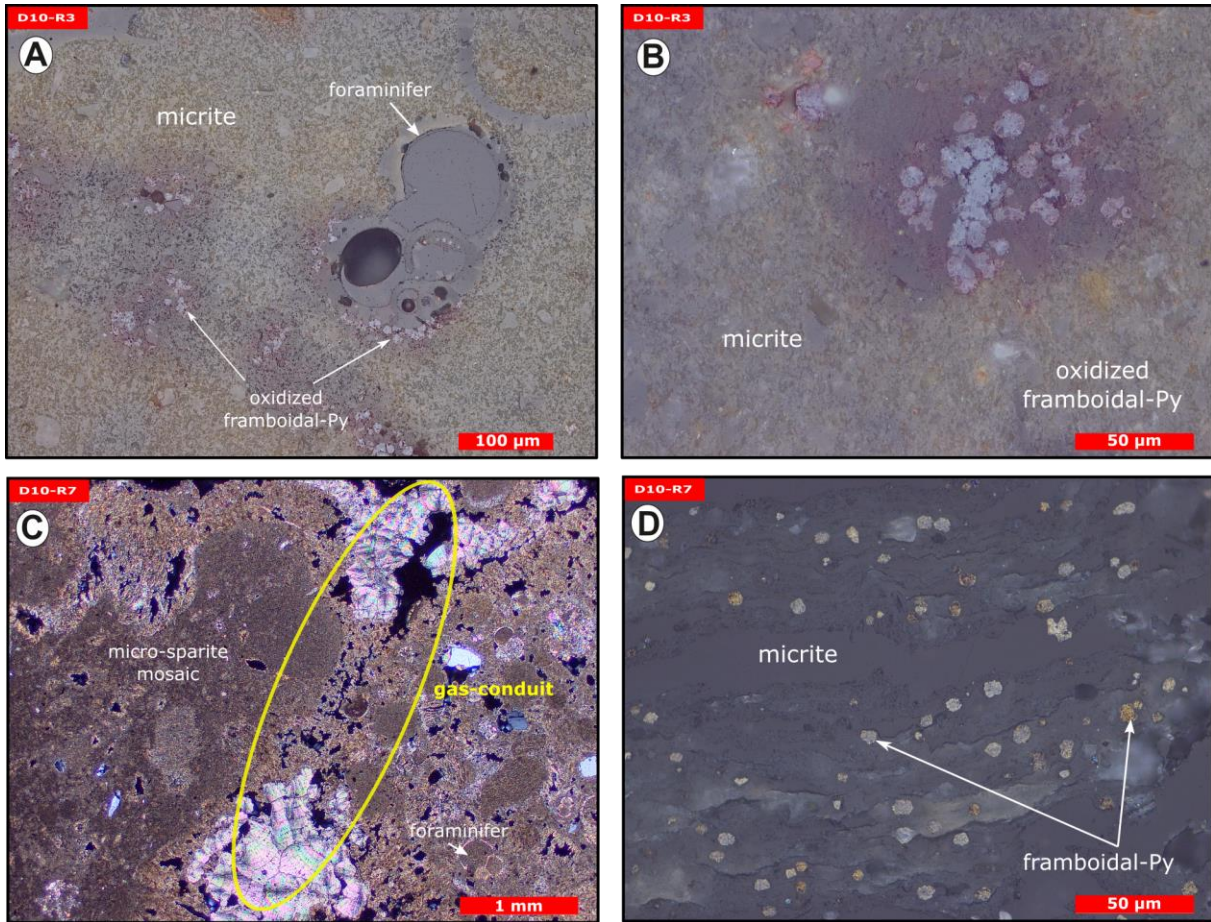
734  
 735  
 736  
 737  
 738  
 739

**Figure 6.** ROV still frames from the Northern Pompeia Coral Ridge and extinct MV (Dive 03), where there is currently a diffused seepage of fluids. **A:** abundant shells of chemosynthetic bivalves with sulfide-oxidizing bacterial mats at the western site of the Northern Pompeia Coral Ridge; **B–D:** field of dead scleractinian-corals colonized by living corals; **D:** still frame from the extinct MV.

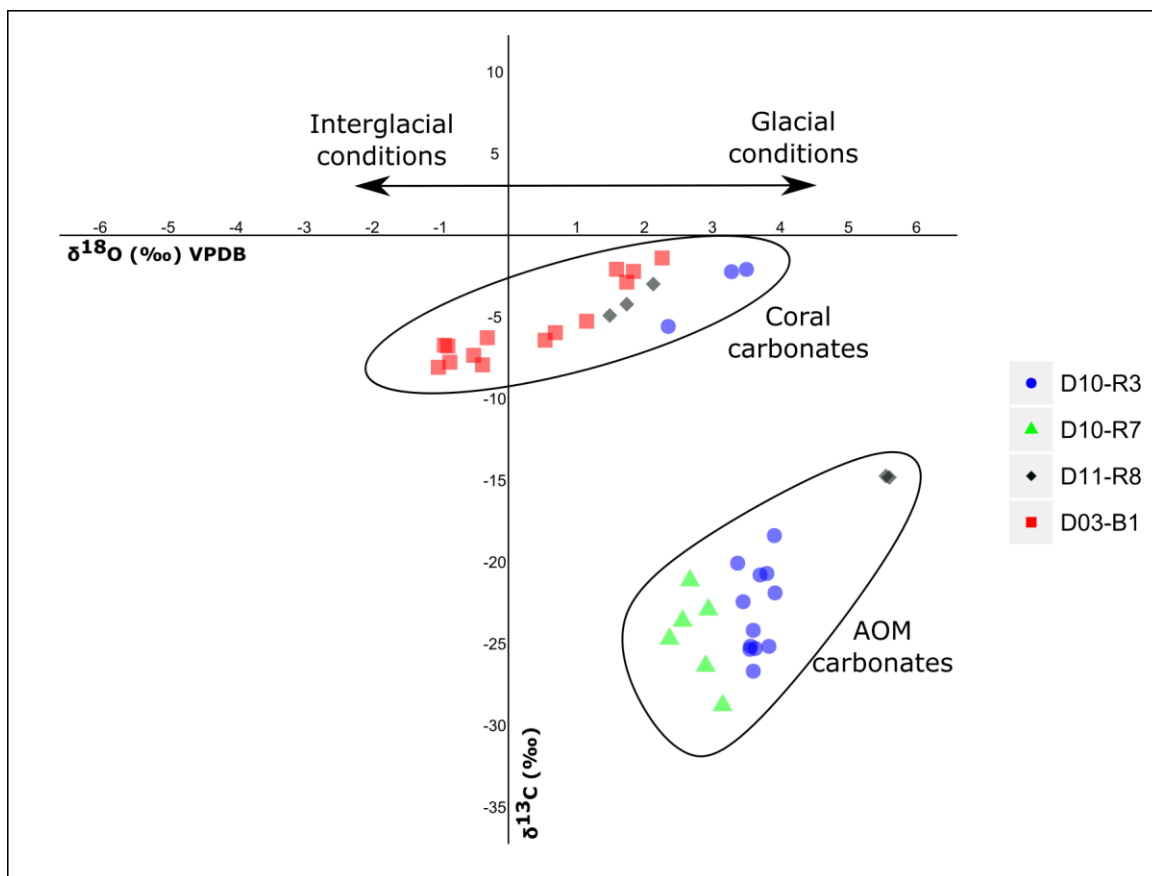


740  
 741  
 742  
 743  
 744  
 745  
 746  
 747

**Figure 7.** Photographs of analyzed samples including sampling sites for stable carbon and oxygen isotope ( $\delta^{13}\text{C}$ ,  $\delta^{18}\text{O}$ ) analysis (crosses with numbers). Values of the stable isotopic analyses are found in **Table 2**. **A–B:** D10-R3 carbonate with embedded corals; **C–D:** D10-R7 carbonate with strong  $\text{H}_2\text{S}$  odor; **E–F:** D11-R8 carbonate with embedded corals; **G:** D03-B1 scleractinian-coral fragment, *Madrepora oculata*.

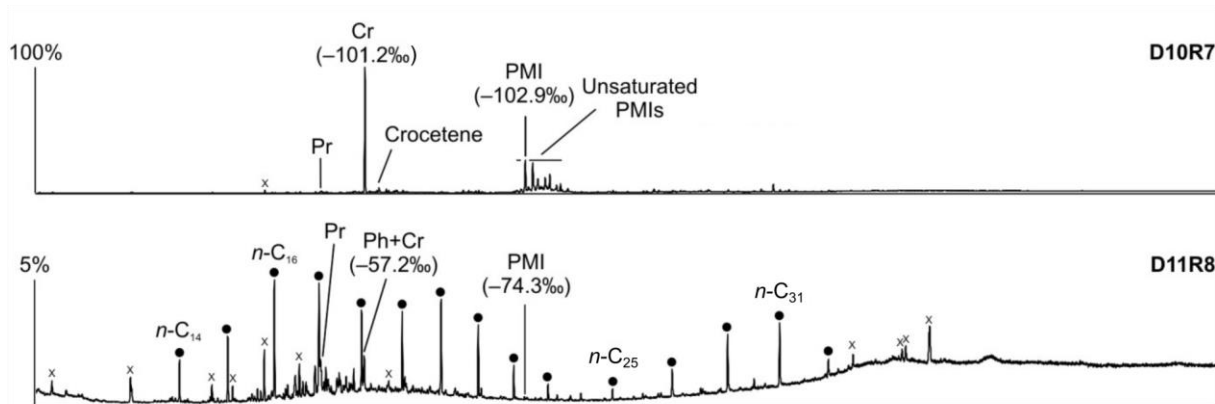


748  
 749 **Figure 8.** Thin section photographs of MDACs. **A–B:** D10-R3 consisting of a micritic matrix with scattered  
 750 foraminifers and oxidized framboidal pyrites (reflected light); **C–D:** D10-R7 consisting of micritic and micro-  
 751 sparitic carbonate with abundant unaltered framboidal pyrites (C, transmitted light; D, reflected light). Please note  
 752 open voids which represent potential pathways for fluid seepage (yellow circle in C).  
 753



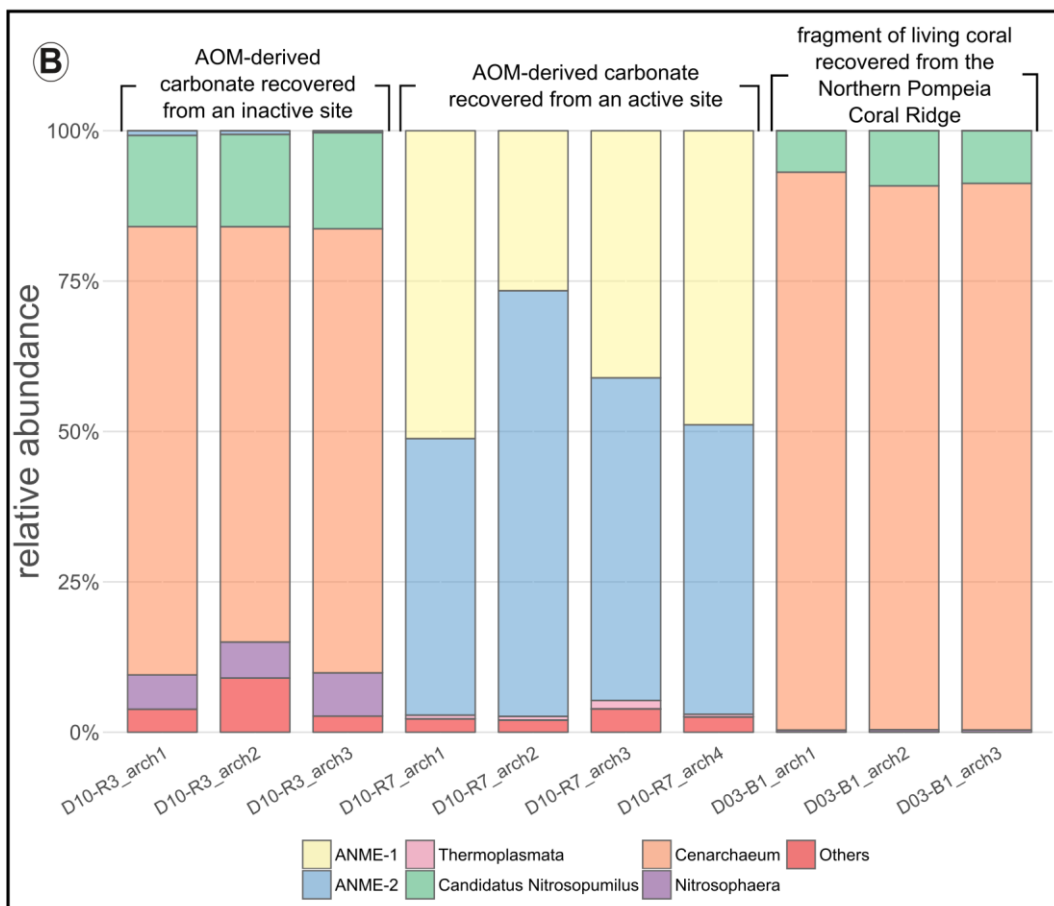
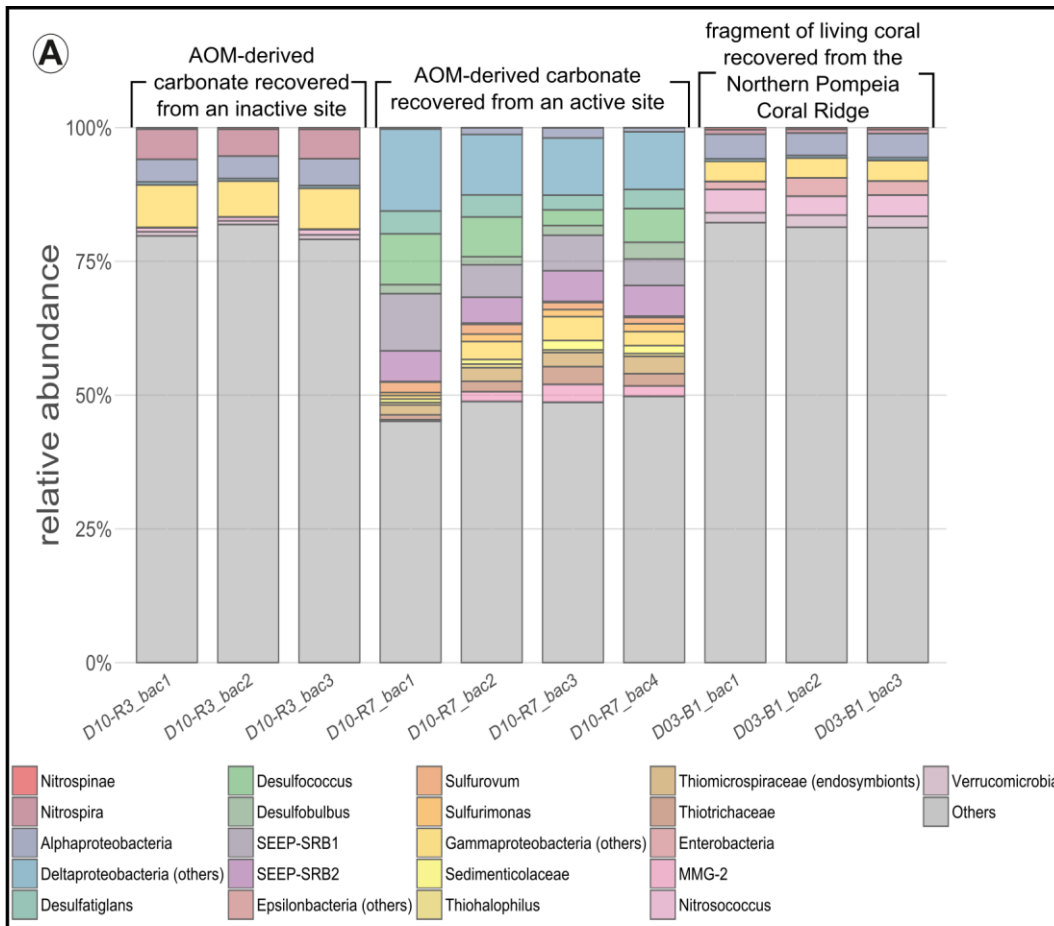
754  
 755 **Figure 9.** Stable carbon and oxygen isotopes ( $\delta^{13}\text{C}$ ,  $\delta^{18}\text{O}$ ) of samples from the Al Gacel MV and the Northern  
 756 Pompeia Coral Ridge (see **Figure 3** for precise sampling points).

757  
 758  
 759  
 760



761  
 762 **Figure 10.** Total ion current (TIC) chromatograms of the analyzed samples. Isotopically depleted acyclic irregular  
 763 isoprenoids such as Cr and PMI are typically found in settings influenced by the anaerobic oxidation of methane  
 764 (AOM). Pr = pristane; Ph = phytane; Cr = crocetane; PMI = 2,6,10,15,19-pentamethylcosane; dots = n-alkanes;  
 765 crosses = siloxanes (septum or column bleeding). Percentage values given on the vertical axes of chromatograms  
 766 relate peak intensities to highest peak (Cr in D10-R7).

767



769 **Figure 11.** Bar charts representing relative abundances of prokaryotic taxa detected in each sample. **A:** bacterial  
770 taxa; **B:** archaeal taxa. In “others” aggrupation is included taxa related to ubiquitous organism normally found in  
771 sea- and seepage-related environments, and unclassified organisms. Number of reads per taxa detailed in **Table**  
772 **S1** (bacteria) and **Table S2** (archaea).

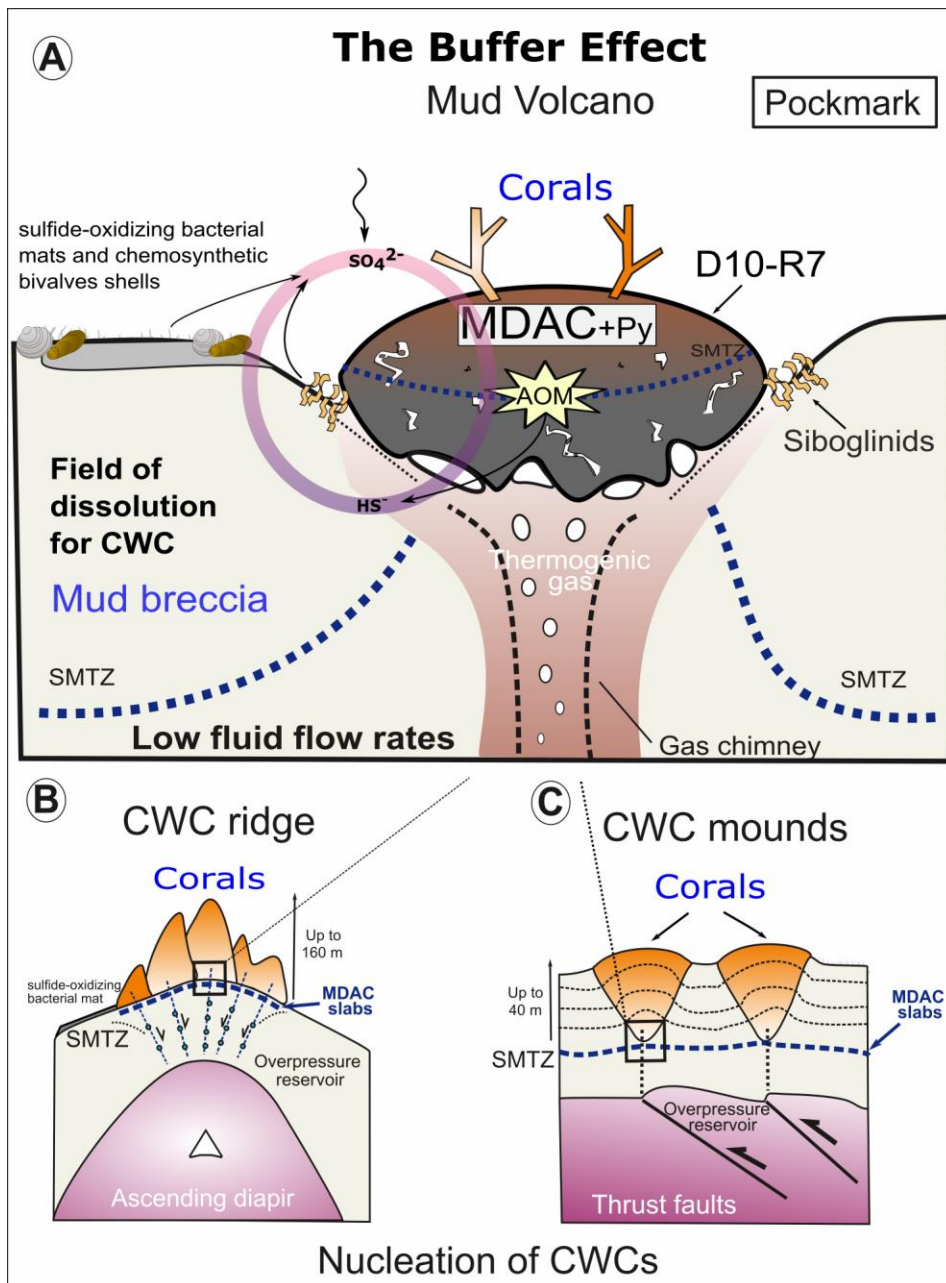


**Figure 12.** The buffer effect model. **A:** Buffer effect at pockmark sites (e.g. sampling site of D10-R7) where carbonates are formed directly on the bubbling site acting as a cap; **B:** Buffer effect at diapiric ridges where MDAC slabs are formed on the base of the ridge; **C:** Buffer effect at coral mounds where MDAC slabs are formed in deeper layers of the sediment. Py = pyrite, SMTZ: sulfur-methane transition zone.

775